Agreement INGV-DPC 2007-2009

Project S4: ITALIAN STRONG MOTION DATA BASE

Responsibles: Francesca Pacor, INGV MIlano – Pavia
and Roberto Paolucci, Politecnico Milano

http://esse4.mi.ingv.it

Deliverable # 6

Application of Surface wave methods for seismic site characterization

May 2009

edited by:

UR4 Sebastiano Foti, Politecnico di Torino

UR8 Stefano Parolai, Helmholtz Centre Potsdam GFZ German Research Centre for Geosciences

UR7 Dario Albarello, Università di Siena

Contributors

UR1 – INGV Milano

Rodolfo Puglia

UR4 – Politecnico di Torino

Cesare Comina (Università di Torino), Sebastiano Foti, Margherita Maraschini, Ken Tokeshi

UR7 – Università di Siena

Dario Albarello

UR8 – Helmholtz Centre Potsdam GFZ German Research Centre for Geosciences

Stefano Parolai, Matteo Picozzi

Table of Contents

1. Description of the Deliverable

This deliverable reports a detailed description of surface wave tests which have been selected as the primary tool for the characterization of the accelerometric stations of the RAN within Project S4, due to their flexibility and cost effectiveness. Within the range of techniques which can be adopted for surface wave testing, the advantage and limitations of active and passive methods are discussed, with special attention to the objective of the project. In this view, the sites to be characterised within the project S4 have been selected accounting also for the technique best suited for surface wave testing at a specific location.

1.1 Introduction

Surface waves have been studied in seismology for the characterization of Earth's interior since the 1920s, but their widespread use started during the 1950s and 1960s thanks to the increased possibilities of numerical analysis and to the improvements of instrumentation for recording seismic events associated to earthquakes (Dziewonski and Hales, 1972; Aki and Richards, 1980; Ben-Menhaem and Sigh, 2000). Geophysical applications at regional scale for the characterization of geological basins make use of seismic signals from explosions (Malagnini et al., 1995) and microtremors (Horike, 1985). Engineering applications started in the 1950s with the Steady State Rayleigh Method (Jones, 1958), but their diffusion arrived only in the last two decades, initially with the introduction of the SASW (Spectral Analysis of Surface Waves) method (Stokoe et al., 1994) and then with the spreading of multistation methods (Foti, 2000). The recent interest in surface waves methods in shallow geophysics is witnessed by workshops and sessions in International Conferences and by dedicated issues of International Journals (EAGE – Near Surface Geophysics, November 2004; Journal of Engineering and Environmental Geophysics, June and September 2005).

Despite the different scales, the aforementioned applications rely on the same basic principles. They are founded on the geometrical dispersion, which makes Rayleigh wave velocity of propagation frequency dependent in vertically heterogeneous media. High frequency (short wavelength) Rayleigh waves propagate in shallow zones close to the free surface and are informative about their mechanical properties, whereas low frequency (long wavelength) components involve deeper layers. Surface wave methods use this property to characterize materials in a very wide range of scales, from microns to kilometres. The essential difference between applications is given by the frequency range of interest and on spatial sampling, as it will be detailed in next sections. Surface wave tests are typically devoted to the determination of a small strain stiffness profile for the site under investigation.

In order to summaries the concept behind the use of geometrical dispersion for soil characterization, let's assume that the stratified medium in Figure 1a is characterized by increasing stiffness with depth, so that the shear wave velocity of the top layer is lower than the velocity of the second layer which in turn is lower than the velocity of the halfspace below. In such situation, a high frequency Rayleigh wave (Figure 1), travelling in the top layer will have a velocity of propagation slightly lower than the velocity of shear wave in the first layer. On the other hand a low frequency wave (Figure 1) will travel at an higher velocity because it is influenced also by the underlying stiffer materials. This concept can be extended to several frequency components. The phase velocity vs. wavelength (Figure 1) plot will hence show an increasing trend for longer wavelength. Considering the relationship between wavelength and frequencies, this piece of information can be represented as a phase velocity

vs frequency plot (Figure 1). This graph is usually addressed as dispersion curve. This example shows, for a given a vertically heterogeneous medium, that the dispersion curve will be associated to the variation of medium parameters with depth. This is the so called forward problem.

If the dispersion curve is estimated on the basis of experimental data, it is then possible to solve the inverse problem, i.e. the model parameters are identified on the basis of the experimental data collected on the boundary of the medium. This is the essence of surface wave methods.

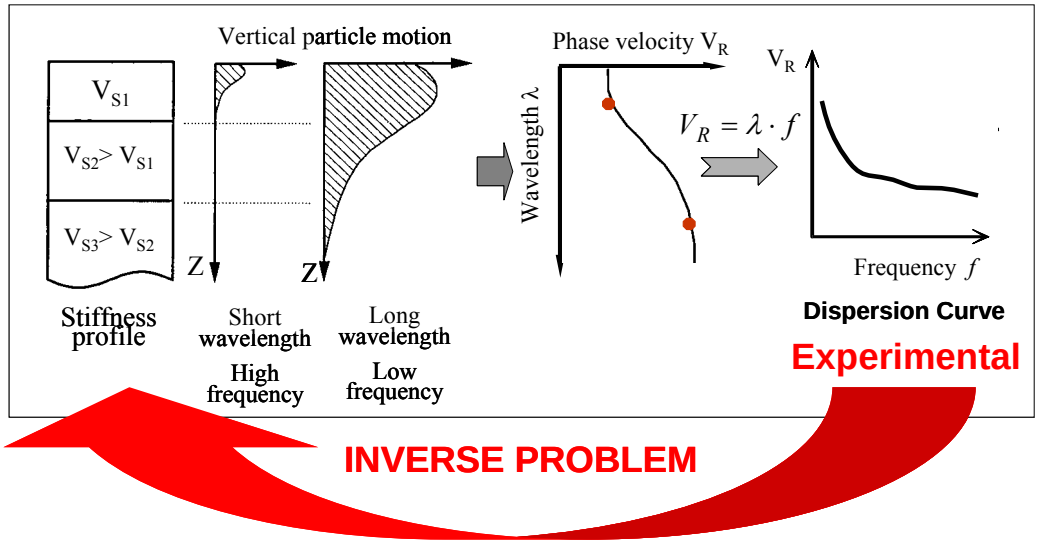

Figure 1 – Parameter identification on the basis of geometrical dispersion

Figure 2 reports the standard procedure for surface wave tests, which can be subdivided into three main steps:

1. acquisition of experimental data;
2. signal processing to obtain the experimental dispersion curve;
3. inversion process to estimate shear wave velocity profile at the site.

It is very important to recognize that the above steps are strongly interconnected and their interaction must be adequately accounted for during the whole interpretation process.

Appealing alternatives for the interpretation of surface wave data are the inversion of field data based on full waveform simulations and the inversion of the Fourier frequency spectra of observed ground motion (Szelwis and Behle, 1987), but these strategies are rarely used because of their complexity. Moreover the experimental dispersion curve is informative about trends to be expected by the final solution, so that its visual inspection is important for the qualitative validation of the results. Indeed engineering judgment plays a certain role in test interpretation. Since the site and the acquisition are never “ideal”, also the results of fully automated interpretation procedures must be carefully examined, with special attention to intermediate results during each step of the interpretation process. A deep knowledge of theoretical aspects and experience are hence essential.

Surface wave data can also be used to characterize the dissipative behaviour of soils. Indeed the spatial attenuation of surface waves is associated to the internal dissipation of energy. Using a procedure substantially analogous to the one outlined in Figure 2, it is possible to extract from field data the experimental attenuation curve, i.e. the coefficient of attenuation of

surface wave as a function of frequency, and then use this piece of information in an inversion process aimed at estimating the damping ratio profile for the site (Lai et al., 2002; Foti, 2004).

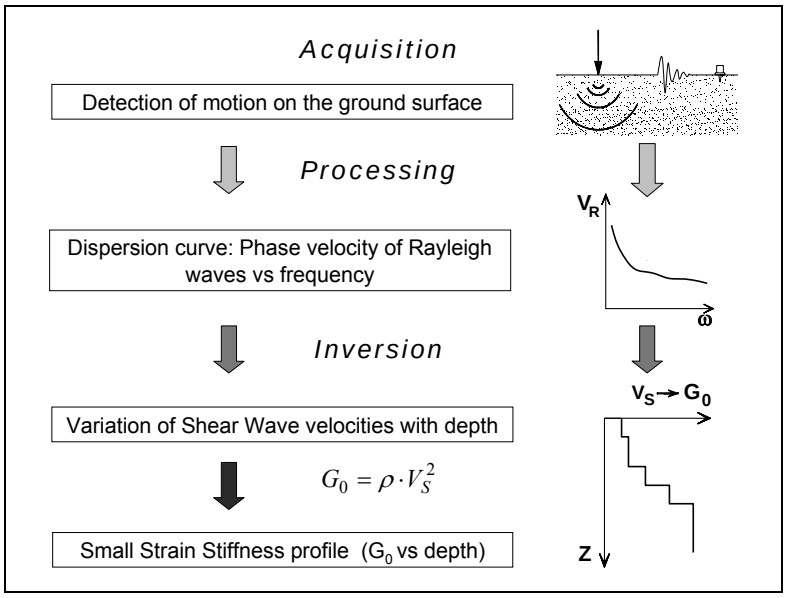

Figure 2 – Flow chart of surface wave tests.

The primary use of surface wave testing is related to site characterization in terms of shear wave velocity profile. The V_S profile is of primary interest for seismic site response studies and for studies of vibration of foundations and vibration transmission in soils. Other applications are related to the prediction of settlements and to soil-structure interaction.

With respect to the evaluation of seismic site response, it is worth noting the affinity between the model used for the interpretation of surface wave tests and the model adopted for most site responses study. Indeed the application of equivalent linear elastic methods is often associated with layered models (e.g. the code SHAKE and all similar approaches). This affinity is also particularly important in the light of equivalence problems, which arise because of non-uniqueness of the solution in inverse problems. Indeed profiles which are equivalent in terms of Rayleigh wave propagation are also equivalent in term of seismic amplification (Foti et al., 2009).

Many seismic building codes introduce the weighted average of the shear wave velocity profile in the shallowest 30m as to discriminate class of soils to which a similar site amplification effect can be associated. The so-called $V_{S,30}$ can be evaluated very efficiently with surface wave method also because its average nature does not require the high level of accuracy that can be obtained with seismic borehole methods (such as Cross-Hole tests and Down-Hole tests).

Several comparison of surface wave test with more accurate methods such as cross-hole tests and down-hole tests are reported throughout the technical and scientific literature, showing the reliability of the method (see for example Figure 3)

A brief discussion of each step involved in surface wave testing is reported in the following, whereas the reader is referred to the relevant sections for details and technical aspects.

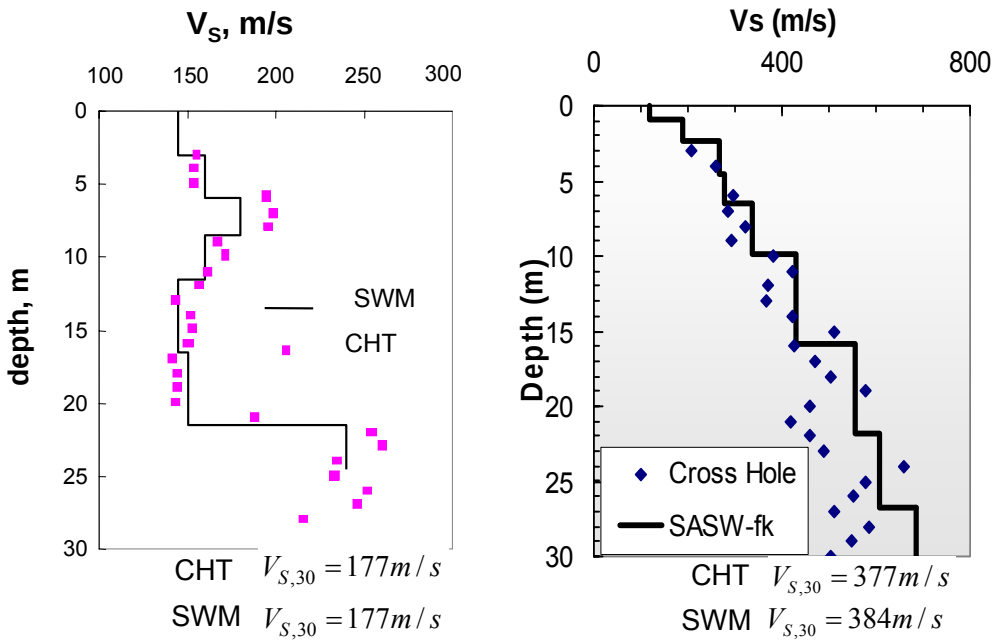

Figure 3 – Comparisons between surface wave tests (SWM) and cross-hole tests in terms of shear wave velocity profile and VS,30: (a) Leaning Tower of Pisa site (Foti, 2003); (b) Saluggia site (Foti, 2000).

Acquisition

Surface wave data are typically collected on the ground surface using a variable number of receivers. Several variations can be introduced both in the choice of receivers and acquisition device and in the generation of the wave fields.

The receivers adopted for testing related to exploration geophysics and engineering near surface applications are typically geophones (velocity transducers). Accelerometers are more often used for characterization of pavement systems because in that case the need of high frequency components makes the use of geophones not optimal.

The advantage of using geophones instead of accelerometers arises because geophones do not need a power supply, whereas accelerometers do. On the other hand low frequency geophones (natural frequency less than 2Hz) tend to be bulky and very vulnerable because the heavy suspended mass can easily be damaged during deployment on site.

Several devices can be used for the acquisition and storage of signals. Basically any device having an A/D converter and the capability to store the digital data can be adopted, ranging from seismograph to dynamic signal analyzers to on purpose acquisition systems built using acquisition boards connected to PCs or laptops. Commercial seismographs for geophysical prospecting are typically the first choice because they are designed to be used in the field, so they are very robust, waterproof and resistant to dust. New generation seismographs are composed by scalable acquisition blocks to be used in connection with field computers, hence allowing preliminary processing of data on site.

As the generation of the wavefield is concerned several different sources can be used, provided they offer sufficient energy in the frequency range of interest for the application. Impact sources are often preferred because they are quite cheap and allow for fast testing. A variety of impacts can be used ranging from small hammers, for the high frequency range, to large falling weights, which generate low frequency components. Appealing alternatives are controlled sources which are able to generate a harmonic wave, hence assuring very high

quality data. Also in this case the size of the source is variable from relatively small electromagnetic shakers to large truck-mounted vibroseis. The drawback of such source is their cost and also the need of longer acquisition processes on site, also if this aspect could be circumvented using swept-sine signals as input.

A different perspective is the use of microtremors analysis. In this case the need for the source is avoided by recording background noise and the test is performed using a "passive" approach. Microtremors are both cultural noise generated by human activities (traffic on highways, construction sites, …) and vibrations associated to natural events (sea waves, wind, etc.). A great advantage is that microtremors are usually rich in low frequency components, whereas high frequency components are strongly attenuated when they travel through the medium and are typically not detected. Hence microtremors survey provide useful information for deep characterization (tens or hundreds of meters), whereas the level of details close to the ground surface is typically low. In microtremor survey, however, the choice of the appropriate instrument is crucial (see e.g. Strollo et al., 2008 and references therein).The limitation in resolution close to the ground surface can be overcome combining active and passive measurements.

Processing

The field data are processed to estimate the experimental dispersion curve, i.e. the relationship between phase velocity and frequency. The different procedures apply a variety of signal analysis tools, mainly based on the Fourier Transform. Indeed using Fourier analysis it is possible to separate the different frequency components of a signal that are subsequently used to estimate phase velocity using different approaches in relation to the testing configuration and the number of receivers.

Some equipments allow for a preprocessing of experimental data directly in the field. Indeed the simple visual screening of time traces is not always sufficient because surface wave components are grouped together and without signal analysis it is not possible to judge quality of data. In particular an assessment of the frequency range with high signal quality can be particularly useful to assess the necessity of changing the acquisition setup or the need for gathering additional experimental data.

Inversion

The solution of the inverse Rayleigh problem is the final step in test interpretation. The solution of the forward problem (Chapter 4) forms the basis of any inversion strategy. Assuming a model for the soil deposit, model parameters are identified minimizing an object function representing the distance between the experimental and the numerical dispersion curves. The object function can be expressed in terms of any mathematical norm (usually the RMS) of the difference between experimental and numerical data points. In practice the set of model parameters which produces a solution of the forward problem (a numerical dispersion curve) as close as possible to the experimental data (the experimental dispersion curve of the site) is selected as solution of the inverse problem (e.g. Figure 4).

This objective can be reached using a variety of strategies. A major distinction arises between Local Search Methods (LSM), which minimize the difference starting from a tentative profile and searching in its vicinity, and Global Search Methods (GSM), which attempt to explore the entire space of possible solutions. LSMs are undoubtedly faster since they requires a limited number of runs of the forward problems of Rayleigh wave propagation, but since the solution

is searched in the vicinity of a tentative profile, there is the risk of being trapped in local minima. On the other side GSMs require a much bigger computational effort since a large number of runs of the forward problem is required, so that the approach is quite time consuming.

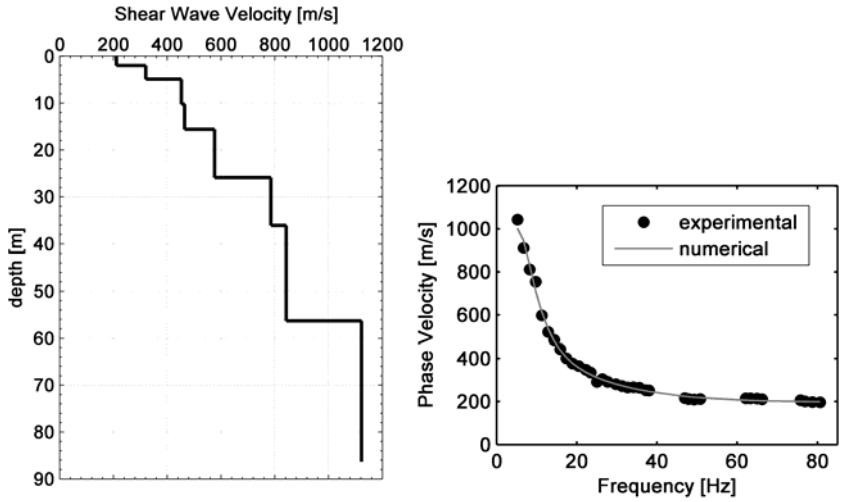

Figure 4 – Example of inversion process: (a) shear wave velocity profile; (b) comparison between the correspondent numerical dispersion curve and the experimental one

In general inverse problems are inherently ill-posed and a unique solution does not exist. A major consequence is the so called equivalence problem, i.e. several shear wave velocity profiles can be equivalent with respect to experimental dispersion curve, meaning that the numerical dispersion curve associated to each of this profile is at the same distance from the experimental dispersion curve. A meaningful evaluation of equivalent profiles has to take into account also the uncertainties in the experimental data. Additional constrains and a priori information from borehole logs or other geophysical tests are useful element to attenuate the equivalence problem.

2. Active source methods

2.1 SASW

The traditional SASW method uses either impulsive sources such as hammers or steady-state sources like vertically oscillating hydraulic or electro-mechanical vibrators that sweep through a pre-selected range of frequencies, typically between 5 and 200 Hz. R-waves are detected by a pair of transducers located at distances D and D+X from the source. The signals at the receivers are digitised and recorded by a dynamic signal analyser. The Fast Fourier Transform is computed for each signal and the cross power spectrum between the two receivers is calculated. Multiple signals are averaged to improve the estimate of the cross power spectrum. An impact source creates a wave-train, which has components in a broad frequency range. The ground motion is detected by a pair of receivers, which are placed along a straight line passing from the source, and the signals are then analysed in the frequency domain. The phase velocity V_R is obtained from the phase difference of the signals using the following relationship:

$$V_R(\omega) = \frac{\omega}{\Theta_{12}(\omega)} \cdot X \qquad (1)$$

in which $\Theta_{12}(\omega)$ is the cross-power spectrum phase, ω is the angular frequency and X is the inter-receiver spacing.

One critical aspect of the above procedure is the influence of signal-to-noise ratio. Indeed the measurement of phase difference is a very delicate task. The necessary check on the signal to noise ratio is usually accomplished using the coherence function (Santamarina and Fratta, 1998), whose value is equal to 1 for linearly correlated signals in absence of noise. Only the frequency ranges having a high value of the Coherence function are used for the construction of the experimental dispersion curve. It must be remarked that the coherence function must be evaluated using several pairs of signals, leading to the necessity of repeating the test using the same receiver setup.

As an example, Figure 5 shows the spectral quantities relative to the couple with 18m spacing, selected from the test performed using the weight-drop source. Together with the Cross-Power Spectrum phase, the Coherence function and the Auto-Power spectra at the two receivers are reported. These other quantities give a clear picture of the frequency range in which the most of energy is concentrated and hence there is a high signal-to-noise ratio.

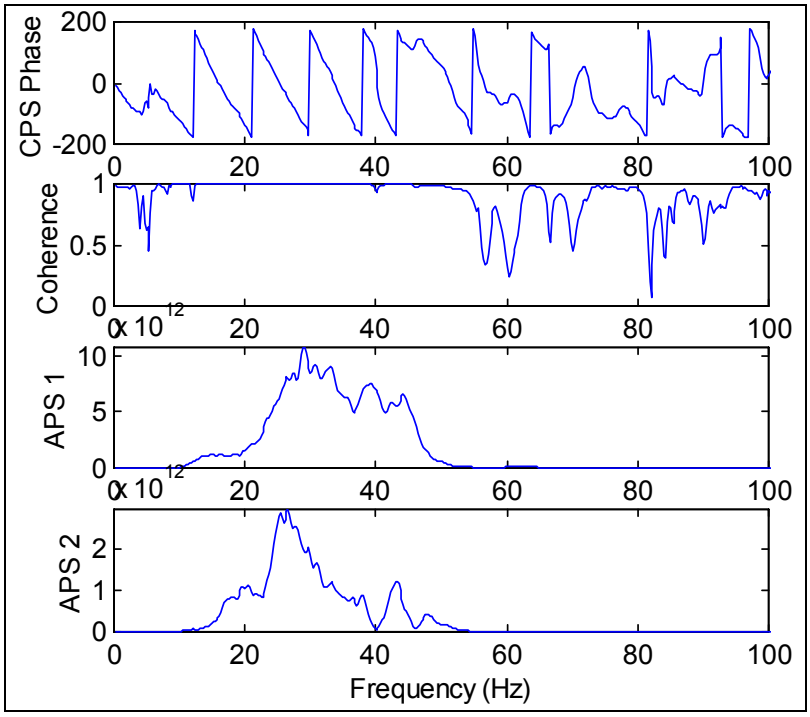

Figure 5 – Example of two-receiver data elaboration (source: 130kg weight-drop, inter-receiver distance 18m): a) cross power spectrum (wrapped); b) coherence function; c) Auto-power spectrum (receiver 1); c) Auto-power spectrum (receiver 2) (Foti, 2000)

Other important concerns are near-field effects and spatial aliasing in the recorded signals. In this respect, usually a filtering criterion (function of the testing setup) is applied to the dispersion data (Ganji et al., 1998). E.g. only frequencies for which the following relationship is satisfied are retained:

$$\frac{X}{3} < \lambda_R(\omega) < 2D \qquad (2)$$

in which $\lambda_R(\omega) = V_R(\omega)/f$ is the estimated wavelength, D is the source-first geophone distance, and X is the inter-receiver spacing (Fig. 1). Typically, the receiver positions are such that X and D are equal, in accordance to the results of some parametric studies about the optimal test configuration (Sanchez-Salinero, 1987).

The above filtering criterion assumes that near fields effects are negligible if the first receiver is placed at least half a wavelength away from the source, for a given frequency in the spectral analysis. Such assumption is acceptable in a normally dispersive site, i.e. a site having stiffness increasing with depth, but it can be optimistic for more complex situations (Tokimatsu, 1995). For this reason and in order to avoid great loss of data, inversion methods that take into account near field effects have been proposed (Roesset et al., 1991, Ganji et al., 1998).

For the aforementioned considerations a single testing configuration gives information only for a particular frequency range, which is dependent on receiver positions. The test is then repeated using a variety of geometrical configurations which include adapting the source type to the actual configuration, i.e. lighter sources (hammers) are used for high frequencies (small receiver spacing) and heavier ones (weight-drop systems) for low frequencies (large receiver spacing). Usually five or six setups are used, moving source and receivers according to a common-receiver-midpoint scheme (Nazarian and Stokoe, 1984).

Typically the test is repeated for each testing configuration in a forward and reverse direction, moving the source from one side to the other with respect to the receivers (Figure 6a). Such procedure is quite time consuming, but it is required to avoid the drift that can be caused by instrument phase shifts between the receivers, since the analysis process is based on a delicate phase difference measurement. Yet, very often the measurements are conducted using a common source scheme (Figure 6b) in order to avoid the need for moving the source, especially when the sources are not easily moved (i.e. large and heavy sources).

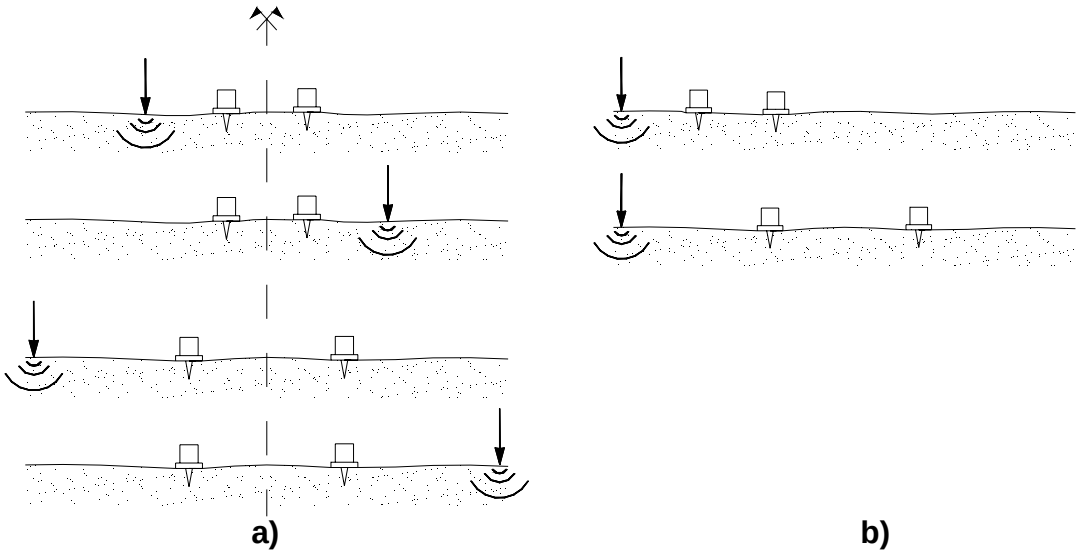

Figure 6 – Acquisition schemes for 2-station SASW: a) common receiver mid-point; b) common source (Foti, 2000)

Finally, the information collected in several testing configurations is assembled (Figure 7) and averaged to estimate the experimental dispersion curve at the site, which will be used for the subsequent inversion process.

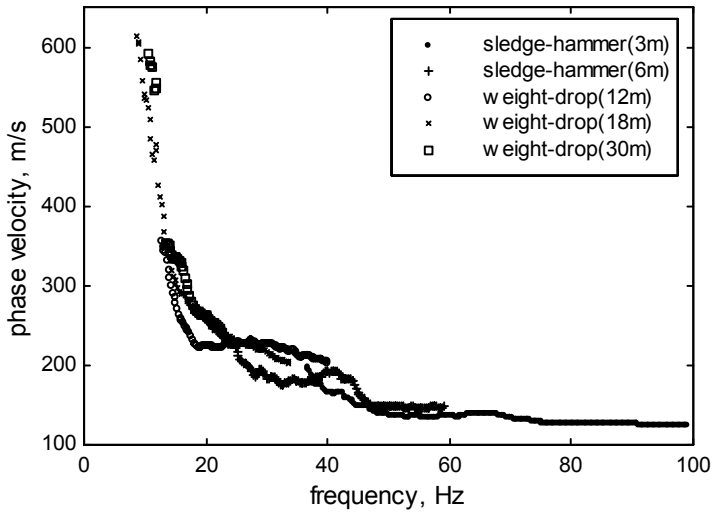

Figure 7 – Assembling dispersion curves branches in SASW method (Foti, 2000)

A very ticklish task in the interpretation of the SASW test is related to the unwrapping of the Cross-Power Spectrum phase. Indeed it is obtained in a modulo-2π, which is very difficult to interpret and unsuitable for further processing (Poggiagliolmi et al., 1982). The passage to an unwrapped (full-phase) curve is necessary for the computation of time delay as a function of frequency (see Equation 1).

Usually some automated algorithms are applied for this task (Poggiagliolmi et al., 1982), but external noise can produce fictitious jumps in the wrapped phase, which drastically damage the results. Not always the operator can correct such unwrapping errors on the basis of judgement and in any case it is a subjective procedure, which precludes the automation of the process. An automated procedure based on a least-square interpolation of the cross-power spectrum phase has also been proposed (Nazarian and Desai, 1993).

2.2 MASW

The use of a multi-station testing setup can introduce several advantages in surface wave testing. In this case, the motion generated by the source is detected simultaneously at several receiver locations in line with the source itself. The experimental data are typically transformed from the time-offset domain to different domains, where the dispersion curve is easily extracted from spectral maxima. For example applying a double Fourier transform to field data the dispersion curve can be identified as the maxima in the frequency-wavenumber panel (Figure 8). Other methods use different transforms obtaining similar results, e.g. the *ω-p* (frequency-slowness) panel obtained with the slant-slack transform (McMechan & Yedlin, 1981) or the MASW method (Park et al., 1999). The formal equivalence of these approaches can be proved considering the mathematical properties of the different transforms (Santamarina & Fratta, 1998) and there is practically no difference in the obtained dispersion curves (Foti, 2000).

In theory transform-based methods allow the identification of several distinct Rayleigh modes. Tselentis and Delis (1998) showed that the *fk* spectrum for surface waves in layered media can be written as the following sum of modal contributions:

$$F(f,k) = \sum_m S_m(f) \cdot \left[\sum_{n=1}^{N} e^{-\alpha_m(f)\cdot x_n} \cdot e^{i(k-k_m(f))\cdot x_n} \right] \qquad (3)$$

where S_m is a source function, x_n is the distance from the source of the n^{th} receiver, α_m and k_m are respectively attenuation and wavenumber for the m^{th} mode. Observing the quantity in square bracket it is evident that, if material attenuation is neglected, the maxima of the energy spectrum are obtained for $k = k_m(f)$. Furthermore it can be shown that also if the above differentiation is conducted without neglecting the material attenuation the conclusion is the same, i.e. the accuracy is not conditioned by material attenuation (Tselentis and Delis 1998).

Once the modal wavenumbers have been estimated for each frequency, they can be used to evaluate the dispersion curve recalling that phase velocity is given by the ratio between frequency and wavenumber.

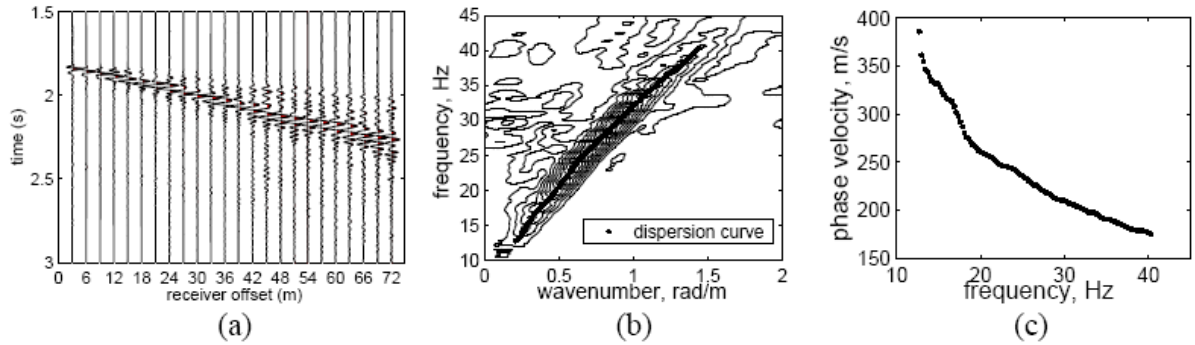

Figure 8 – Example of processing of experimental data using the frequency-wavenumber analysis: (a) field data; (b) fk panel; (c) dispersion curve (Foti, 2005)

Using a very large number of signals (256) Gabriels et al. (1987) were able to identify six experimental Rayleigh modes for a site and then they used these modes for the inversion process. The possibility of using modal dispersion curves is a great advantage with respect to methods giving only a single dispersion curve (as the two-station method) because having more information means a better constrained inversion. Nevertheless it has to be considered that in standard practice the number of receivers for engineering applications is typically small and reduced spatial sampling strongly affects the resolution of surface wave test. Receiver spacing influences aliasing in the wavenumber domain, so that if high frequency components are to be sought spacing must be small. On the other side, the total length of the receiver array influences the resolution in the wavenumber domain. Obviously using a finite number of receivers this aspect generates a trade-off similar to the one existing between resolution in time and in frequency. Indeed the resolution in the wavenumber domain is inversely proportional to the total length of the acquisition array. Using a simple 2D Fourier Transform on the original dataset to obtain the experimental fk panel would lead to a spatial resolution not sufficient to obtain a reliable estimate of the dispersion curve. The use of zero padding or the use of advanced spectral analysis techniques such as beamforming or MUSIC (Zwicki, 1999) apparently makes it possible to locate the correct position of the maxima in the fk panel (Figure 9).

Unluckily these strategies do not improve the real resolution, hence it is not possible to separate modal contributions when more than a single mode plays a relevant role in the propagation (Foti et al., 2000). This aspect is exemplified in Figure 10 where slices of the fk spectrum for a given frequency are reported for two different synthetic dataset. If a large number of receivers is used to get evaluate the fk spectrum, the resolution is very high and the energy peaks are well defined, but if the number of receivers is low the resolution is very poor. With poor resolution it is only possible to locale a single peak in the fk panel, which in principle is not associated to a single mode but to several superposed modes. The concept of

apparent phase velocity has been introduced to denote the velocity of propagation corresponding to this single peak representing several modes (Tokimatsu, 1995). In the example of Figure 10a the fundamental mode is the dominant mode in the propagation, meaning that almost all energy is associated to this mode. In this situation the apparent phase velocity is the phase velocity associated to the fundamental mode and the inversion process can be simplified inverting the apparent dispersion curve as a fundamental mode. This situation is usual in soil deposit with stiffness always increasing with depth with no marked impedance jumps between different layers. On the contrary in the example of Figure 10b the fundamental mode is still the one carrying more energy, but it is not anymore dominant, meaning that higher mode plays a relevant role in the propagation. If few receivers are used a single peak will be observed and a single value of phase velocity will be obtained. This value is not necessarily the phase velocity of one of the modes involved in the propagation, but it is rather a sort of average value, often referred as apparent phase velocity or effective phase velocity (Tokimatsu, 1995). In this case it is not anymore possible to use inversion processes based on the fundamental mode or on modal dispersion, but it is necessary to use algorithm that can account for mode superposition effects (Lai, 1998) and for the actual testing configuration (O'Neill, 2004). This situation is usual when strong impedance contrasts are present in the soil profile or in inversely dispersive profiles, i.e. profiles in which soft layers underlie stiff layers.

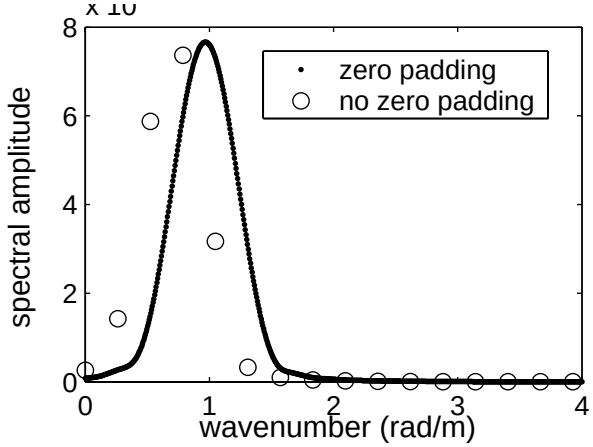

Figure 9 – Effect of zero padding on resolution in the wavenumber domain: slice of the fk panel for a given frequency (Foti, 2000).

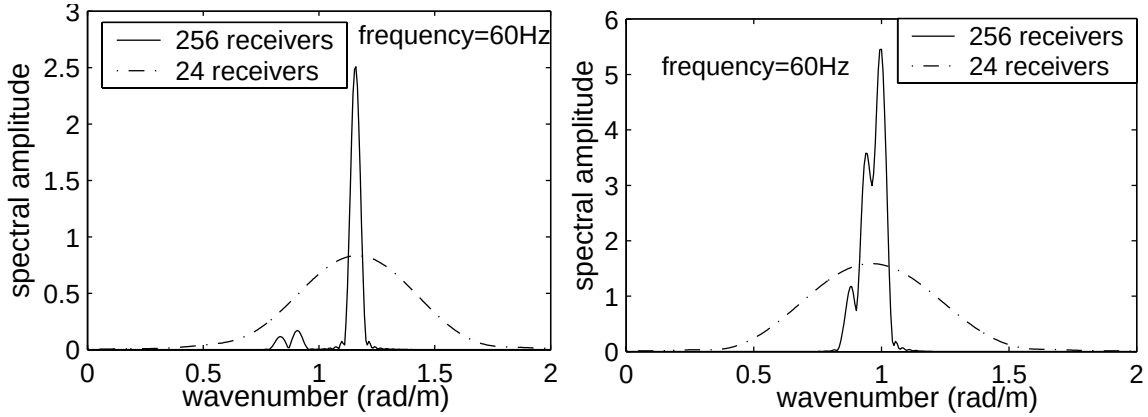

Figure 10 – Influence of the effective wavenumber resolution on the dispersion curve (a) dominant fundamental mode (b) relevant higher modes (Foti, 2000)

The dispersion curves obtained with fk analysis on the synthetic dataset used for Figure 10b are reported in Figure 11. As explained above if a sufficiently high number of receivers is used, it will be possible to obtain the modal dispersion curves (Figure 11a), whereas with the number of receivers used in standard practice a single apparent dispersion curve will be obtained (Figure 11b).

As mentioned above, the apparent dispersion curve is dependent on the spatial array so that if higher modes are relevant for a given site the inversion process will be cumbersome. On the other side if the fundamental mode is dominant, the inversion process can be noticeably simplified. Unluckily, it is not always clear from the simple inspection of the experimental dispersion curve if higher modes are involved.

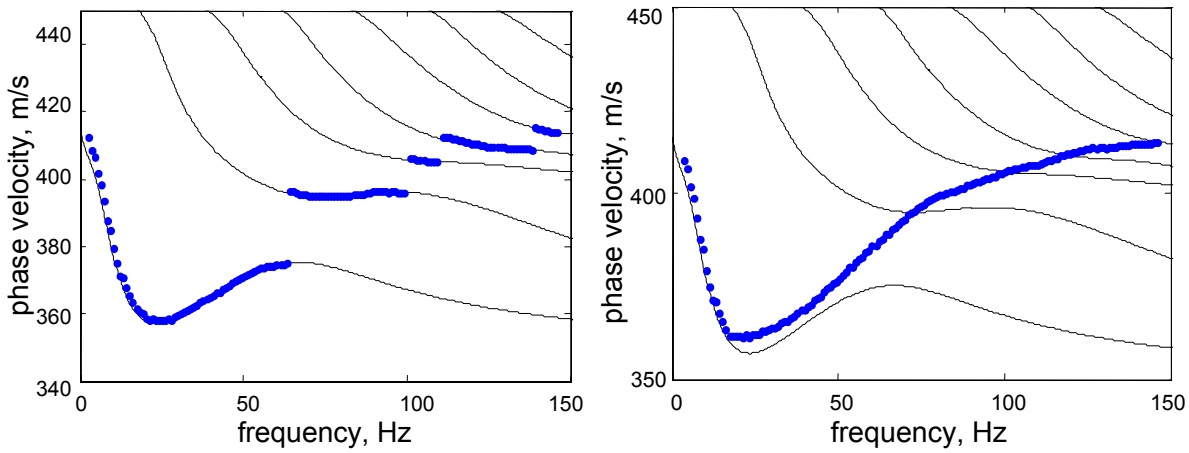

Figure 11 – Influence of wavenumber resolution on the dispersion curve from synthetic data: (a) 256 receivers; (b) 24 receivers (Foti, 2000)

3. Passive source methods

3.1 ReMi

Similarly to the MASW method the multi-station approach can be applied to microtremor recordings. This technique, generally known as Refraction Microtremors (ReMi) was recently introduced by Louie (2001) who proposed as a basis for the velocity spectral analysis the p-tau transformation, or "slantstack", described by Thorson and Claerbout (1985). This transformation takes a record section of multiple seismograms, with seismogram amplitudes relative to distance and time (x-t), and converts it to amplitudes relative to the ray parameter *p* (the inverse of apparent velocity) and an intercept time *tau*. It is familiar to array analysts as "beam forming", and has similar objectives to a two-dimensional Fourier-spectrum or "F-K" analysis as described by Horike (1985).

The p-tau transform is a simple line integral across a seismic record $A(x,t)$ in distance x and time t:

$$A(p,tau) = \int_x A(x,t=tau+p\,x)\,dx \qquad (4)$$

where the slope of the line $p = dt/dx$ is the inverse of the apparent velocity V_a in the x direction. In practice x is discretized into nx intervals at a finite spacing dx , so $x = j\,dx$ with an integer j. Likewise time is discretized with $t = i\,dt$ (with dt usually 0.001-0.01 second),

giving a discrete form of the p-tau transform for negative and positive $p = p0+l\ dp$ and $tau = k\ d\ t$ called the slantstack:

$$A(p=p0+l\ dp,tau=k\ dt) = \sum_{j=0,nx-1} A(x=j\ dx,t=i\ dt=tau+p\ x) \quad (5)$$

starting with a $p0 = -p_{max}$. p_{max} defines the inverse of the minimum velocity that will be found, *np* is effectively set to be one to two times *nx*. *dp* may range from 0.0001-0.0005 sec/m, and is set to cover the interval from $-p_{max}$ to p_{max} in *2np* slowness steps. This will analyze energy propagating in both directions along the refraction receiver line. Amplitudes at times $t = tau+p\ x$ falling between sampled time points are estimated by linear interpolation.

The distances used in refraction microtremor analysis are simply distances of geophones from one end of the array. As described by Thorson and Claerbout (1985), the traces do not have to sample distance evenly, so the straight arrays analyzed here are for the convenience of field layout, not for the convenience of analysis. The intercept times after transformation are thus simply arrival times at one end of the array.

The p-tau transformed records contain, generally 24 or 48 slowness traces, one or more per offset trace in the original x-t records. Each of these traces contains the linear sum across a record at all intercept times, at a single slowness or velocity value. The next step takes each p-tau trace in $A(p,tau)$ (equation5) and computes its complex Fourier transform $F_A(p,f)$ in the tau or intercept time direction:

$$F_A(p,f) = \int_{tau} A(p,tau) e^{-i\ 2\ pi\ f\ tau} dtau \quad (6)$$

for which the discrete Fourier Transform with $f = m\ df$ is:

$$F_A(p,f=m\ df) = \sum_{k=0,nt-1} A(p,tau=k\ dt) e^{-i\ 2\ pi\ m\ df\ k\ dt} \quad (7)$$

although in practice the Fast Fourier Transform is mathematically equivalent but more efficient. Note that this is a one-dimensional transform that does not affect the slowness or *p* axis.

The power spectrum $S_A(p,f)$ is the magnitude squared of the complex Fourier transform:

$$S_A(p,f) = F_A^*(p,f)\ F_A(p,f) \quad (8)$$

where the * denotes the complex conjugate. This method sums together two p-tau transforms of a record, in both forward and reverse directions along the receiver line. To sum energy from the forward and reverse directions into one slowness axis that represents the absolute value of *p*, $|p|$, the slowness axis is folded and summed about p=0 with:

$$S_A(|p|,f) = [\ S_A(p,f)\ ]_{p\geq 0} + [\ S_A(-p,f)\ ]_{p<0} \quad (9)$$

This completes the transform of a record from distance-time (x-t) into p-frequency (p-f) space. The ray parameter p for these records is the horizontal component of slowness (inverse velocity) along the array. In analyzing more than one record from a refraction microtremor deployment the individual records' p-f images $S_{An}(|p|,f)$ are added point-by-point into an image of summed power:

$$S_{total}(|p|,f) = \sum_n S_{An}(|p|,f) \quad (10)$$

So the slowness-frequency analysis has produced a record of the total spectral power in all records from a site, which plots within slowness-frequency (p-f) axes. If one identifies trends within these axes where a coherent phase has significant power, then the slowness-frequency picks can be plotted on a typical period-velocity diagram for dispersion analysis. The p-tau transform is linear and invertible, and can in fact be completed equivalently in the spatial and temporal frequency domains (Thorson and Claerbout, 1985). The use of linear geophone arrays in this technique means that an interpreter cannot just pick the phase velocity of the largest spectral ratio at each frequency as a dispersion curve, as MASW analyses effectively

do. An interpreter must try to pick the lower edge of the lowest-velocity but still reasonable peak ratio. Since the arrays are linear and do not record an on-line triggered source, some noise energy will arrive obliquely and appear on the slowness-frequency images as peaks at apparent velocities V_a higher than the real in-line phase velocity v. In the presence of an isotropic or weakly heterogeneous wave field, it can be demonstrated (Louie, 2001; Mulargia and Castellaro, 2008) that out-of-line wave fronts do not affect significantly the Rayleigh waves dispersion curve. However, this is not true when markedly directional effects exist.

Example of application of the ReMi technique can be found in Stephenson et al. (2005) and Richwalski et al. (2007).

3.2 2D arrays

Seismic arrays were originally proposed at the beginning of the 1960s as a new type of seismological tool for the detection and identification of nuclear explosion (Frosch and Green, 1966). Since then, seismic arrays have been applied at various scales for many geophysical purposes. At the seismological scale, they were used to obtain refined velocity models of the Earth's interior (e.g., Birtill and Whiteway, 1965; Whiteway, 1966; Kværna, 1989; Kárason and van der Hilst, 2001; Ritter et al., 2001; Krűger et al., 2001). A recent review on array applications in seismology can be found in Douglas (2002) and in Rost and Thomas (2002). At smaller scales, since the pioneering work of Aki (1957), seismic arrays have been used for the characterization of surface wave propagation, and the extraction of information on the shallow subsoil structure (i.e. the estimation of the local S-wave velocity profile). Especially in the last decades, due to the focus of seismologists and engineers on estimating the amplification of earthquake ground motion as a function of local geology, and the improvements in the quality and computing power of instrumentation, interest in analyzing seismic noise recorded by arrays (e.g. Horike, 1985; Hough et al., 1992; Ohori et al., 2002; Okada, 2003; Scherbaum et al. 2003, Parolai et al., 2005) has grown.

3.2.1 f-k based methods

The phase velocity of the surface waves can be extracted from noise recordings by using different methods. Here we will illustrate the two most frequently used methods for F-K (frequency-wavenumber) analysis: the Beam-Forming Method (BFM) (Lacoss et al., 1969) and the Maximum Likelihood Method (MLM) (Capon, 1969).

The estimate of the F-K spectra $P_b(f,\mathrm{k})$ by the BFM is given by:

$$P_b(f,k) = \sum_{l,m=1}^{n} \phi_{lm} \exp\{ik(X_l - X_m\} \quad , \tag{11}$$

where f is the frequency, k the two-dimensional horizontal wavenumber vector, n the number of sensors, ϕ_{lm} the estimate of the cross-power spectra between the l^{th} and the m^{th} data, and X_i and X_m, are the coordinates of the l^{th} and m^{th} sensors, respectively.

The MLM gives the estimate of the F-K spectra $P_m(f,\mathrm{k})$ as:

$$P_m(f,k) = \left(\sum_{l,m=1}^{n} \phi_{lm}^{-1} \exp\{ik(X_l - X_m\} \right)^{-1} \quad . \tag{12}$$

Capon (1969) showed that the resolving power of the MLM is higher than that of the BFM, however, the MLM is more sensitive to measurement errors.

From the peak in the F-K spectrum occurring at coordinates k_{xo} and k_{yo} for a certain frequency f_0, the phase velocity c_0 can be calculated by:

$$c_0 = \frac{2\pi f_0}{\sqrt{k_{xo}^{\ 2} + k_{yo}^{\ 2}}} \quad . \tag{13}$$

An extensive description of these methods can be found in Horike (1985) and Okada (2003).

The estimate EP_b and EP_m of the true P_b and P_m *f-k* spectra may be considered the convolution of the true functions with a frequency window function W_f and the wavenumber window functions W_B and W_M for the BFM and MLM, respectively (Lacoss *et al.*, 1969). The first window function W_f is the transfer function of the tapering function applied to the signal time windows (Kind, 2005). The function W_B, is referred differently by various authors (e.g. *spatial window function*" by Lacoss et al., 1969, and "*beam-forming array response function*" by Capon, 1969), and hereafter is defined simply as Array Response Function (ARF). The ARF depends only on the distribution of stations in the array, and for the wavenumber vector k_o has the form (Horike, 1985)

$$W_B\left(k,k_o\right) = \frac{1}{n^2}\sum_{l,m=1}^{n} \exp\left\{i\left(k-k_o\right)\left(X_l - X_m\right)\right\} \tag{14}$$

Simply speaking, it represents a kind of spatial filter for the wavefield. The main advantage of the MLM with respect to the BFM involves the use of an improved wavenumber window W_M. Namely, for a wavenumber k_0 this window function may be expressed in the form

$$W_M\left(f,k,k_0\right) = \left|\sum_{j=1}^{N} A_j\left(f,k_0\right)\right| W_B\left(k,k_0\right) \tag{15}$$

Where

$$A_j\left(f,k_0\right) = \frac{\sum_{l=1}^{N} q_{jl}\left(f,k_0\right)}{\sum_{j,l=1}^{N} q_{jl}\left(f,k_0\right)} \tag{16}$$

and where q_{jl} represents the elements of the cross-power spectral matrix. It is evident that W_M depends not only on the array configuration, through the function W_B, but also on the quality (i.e., signal-to-noise ratio) of the data (Horike, 1985). In fact, the wavenumber response is modified by using the weights A_j (f, k0), which depend directly on the elements $q_{lj}(f)$. In practice, W_M allows the monochromatic plane wave travelling at a velocity corresponding to the wavenumber k_0 to pass undistorted, while it suppresses, in an optimum least-square sense, the power of those waves travelling with velocities corresponding to wavenumbers other than k_0 (Capon, 1969). Or, in other words, coherent signals are associated with large weights of A_j and their energy is emphasized in the *f-k* spectrum. On the contrary, if the coherency is low, the weights A_j are small and the energy in the *f-k* spectrum is damped (Kind et al., 2005). This automatic change of the main-lobe and side-lobe structure for minimizing the leakage of power from the remote portion of the spectrum has a direct positive effect on the P_m function, and consequently on the following velocity analysis. However, considering the dependence of W_M on W_B, it is clear that the array geometry is a factor having a strong influence on both EP_b and EP_m. In fact, similarly to every kind of filter, several large side lobes located around the major central peak can remain in the *f-k* spectra (Okada, 2003) and determine serious biases in the velocity and back-azimuth estimates. In particular, side-lobe height and main-lobe width within W_B control the leakage of energy and resolution, respectively (Zywicki, 1999).

As a general criterion, the error in the velocity analysis due to the presence of spurious peaks in the *f-k* spectra may be reduced using distributions of sensors for which the array response approaches a two-dimensional δ-function. For that reason, it is considered a good practice to undertake a preliminary evaluation of the array response when the survey is planned. Irregular configurations of even only a few sensors should be preferred, because they allow one to obtain a good compromise between a large aperture, which is necessary for sharp main peaks in the EP_b and EP_m, and small inter-sensor distances, which are needed for large aliasing periods (Kind et al., 2005).

Figure 12 shows examples of 2D-array configurations and their respective array responses (Parolai et al., 2007). Figure 13 shows an example of F-K analysis results for 2.5 Hz, 3.9 Hz, and 6.5 Hz for the arrays of Figure 12. White dots indicate the position of the maximum used to estimate the phase velocity while the white circle joins points with the same k values.

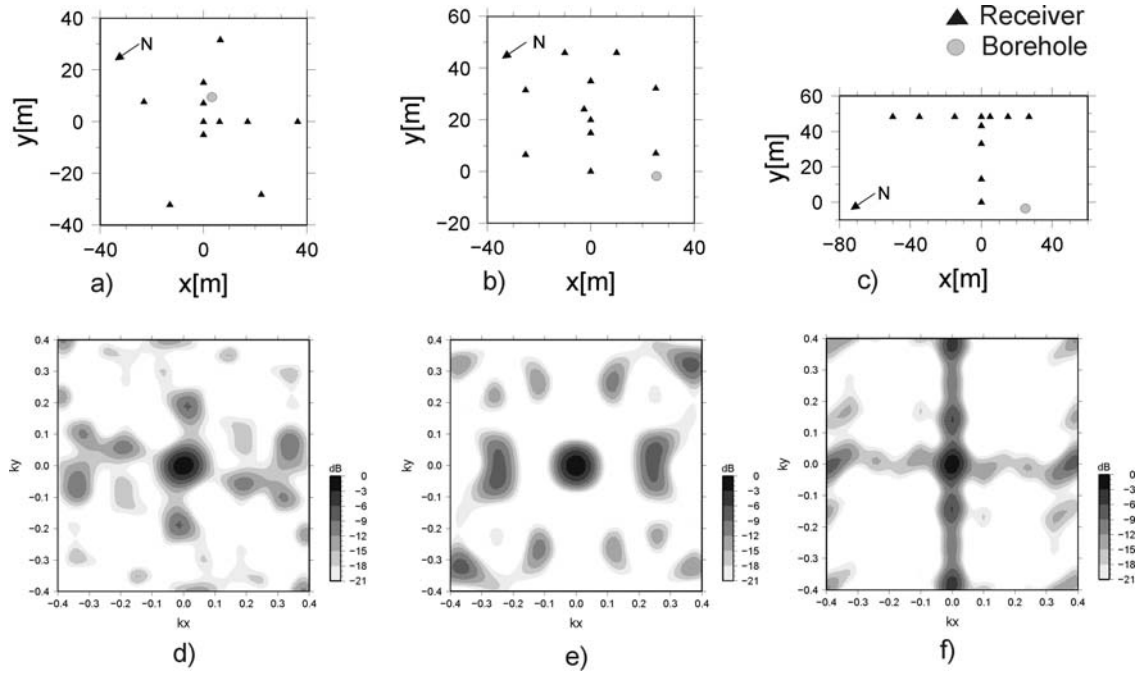

Figure 12 – Top: Examples of micro-array configurations. Bottom: Examples of the relevant micro-array responses. a) Array 1; b) Array 2; c) Array 3. The gray filled circle indicate the borehole location at the Tito test site (Parolai et al., 2007).

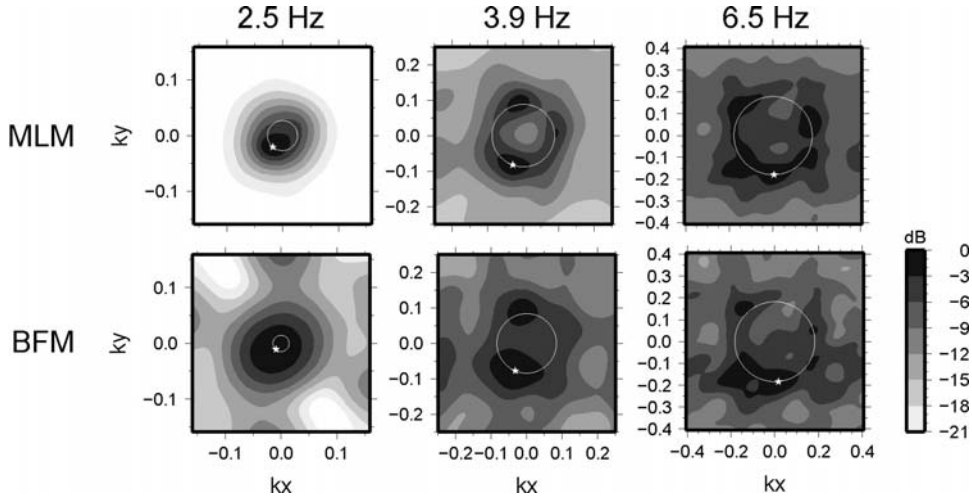

Figure 13 – Example of results from F-K analysis s for 2.5 Hz, 3.9 Hz, and 6.5 Hz. White dots indicate the position of the maximum used to estimate the phase velocity. The white circle joins points with the same k

3.2.2 SPAC and ESAC

Aki (1957,1965) showed that phase velocities in sedimentary layers can be determined using a statistical analysis of ambient noise. He assumed that noise represents the sum of waves propagating without attenuation in a horizontal plane in different directions with different powers, but with the same phase velocity for a given frequency. He also assumed that waves with different propagation directions and different frequencies are statistically independent. Then, a spatial correlation function can be defined as

$$\phi(r,\lambda) = < u(x,y,t)(x + r\cos(\lambda), y + r\sin(\lambda), t) > \quad (17)$$

where $u(x, y, t)$ is the velocity observed at point (x,y) at time t; r is the inter-station distance; λ is the azimuth and $< >$ denotes the ensemble average. An azimuthal average of this function is given by

$$\phi(r) = \frac{1}{\pi}\int_0^{\pi} \phi(r,\lambda)d\lambda \quad . \quad (18)$$

For the vertical component, the power spectrum $\phi(\omega)$ can be related to $\phi(r)$ via the zeroth order Hankel transform

$$\phi(r) = \frac{1}{\pi}\int_0^{\infty} \phi(\omega)J_0\left(\frac{\omega}{c(\omega)}r\right)d\omega \quad , \quad (19)$$

where ω is the angular frequency, $c(\omega)$ is the frequency-dependent phase velocity, and J_0 is the zero order Bessel function. The space-correlation function for one angular frequency ω_0, normalized to the power spectrum, will be of the form

$$\phi(r,\omega_o) = J_0\left(\frac{\omega_0}{c(\omega_0)}r\right) \quad . \quad (20)$$

By fitting the azimuthally averaged spatial correlation function obtained from measured data to the Bessel function, the phase velocity $c(\omega_0)$ can be calculated. A fixed value of r is used in the spatial autocorrelation method (SPAC). However, Okada (2003) and Ohori et al. (2002) showed that, since $c(\omega)$ is a function of frequency, better results are achieved by fitting the spatial-correlation function at each frequency to a Bessel function, which depends on the inter-station distances (extended spatial autocorrelation, ESAC). Therefore, we used this approach in our study.

For every couple of stations the function $\phi(\omega)$ can be calculated in the frequency domain by means of (Malagnini et al., 1993; Ohori et al., 2002; Okada, 2003):

$$\phi(\omega) = \frac{\frac{1}{M}\sum_{m=1}^{M}\mathrm{Re}\left({}_mS_{jn}(\omega)\right)}{\sqrt{\frac{1}{M}\sum_{m=1}^{M}{}_mS_{jj}(\omega)\sum_{m=1}^{M}{}_mS_{nn}(\omega)}} \quad , \quad (21)$$

where ${}_mS_{jn}$ is the cross-spectrum for the mth segment of data, between the jth and the nth station; M is the total number of used segments. The power spectra of the mth segments at station j and station n are ${}_mS_{jj}$ and ${}_mS_{nn}$, respectively.

The space-correlation values for every frequency are plotted as a function of distance, and an iterative grid-search procedure can be then performed using equation (20) in order to find the value of $c(\omega_0)$ that gives the best fit to the data. The tentative phase velocity $c(\omega_0)$ is generally varied over large intervals (e.g. between 100 and 3000 m/s) in small steps (e.g.1 m/s). The

best fit is achieved by minimizing the root mean square (RMS) of the differences between the values calculated with equation (21) and (20). Data points, which differ by more than two standard deviations from the value obtained with the minimum-misfit velocity, can be removed before the next iteration of the grid-search. Parolai et al., (2006) using this procedure allowed a maximum of three grid-search iterations. An example of the application of this procedure for the data set collected in Bevagna is shown in Figure 14. The noise data recordings at each station were divided into 46 windows, each 60 s long.

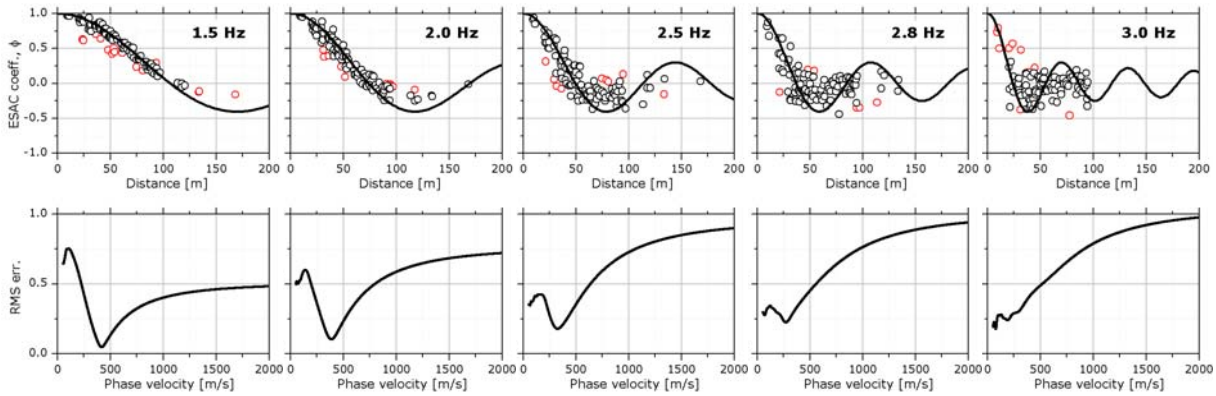

Figure 14 – Top: Measured space-correlation function values (circles) for different frequencies at the Bevagna test site and best-fitting Bessel function (black line). Red circles indicate values discarded by the iterative grid-search procedure, because they lie outside two standard deviations. Bottom: The respective RMS error versus phase velocity curves.

The ESAC method was adopted to derive the phase velocities for all frequencies composing the Fourier spectrum of the data. Figure 14 (top) shows four examples of the space-correlation values computed from the data together with the Bessel function they fit best to; below the corresponding RMS errors as function of the tested phase velocities are shown, exhibiting clear minima. For high frequencies, the absolute minimum sometimes corresponds to the minimum velocity chosen for the grid search procedure. This solution is then discarded, because a smooth variation of the velocity between close frequencies is required. At frequencies higher than a certain threshold the phase velocity might increase linearly. This effect is due to spatial aliasing limiting the upper bound of the usable frequency band. It depends on the S-wave velocity structure at the site and the minimum inter-station distance. At low frequencies (around 1.5 Hz for this test site) the RMS error function quite clearly indicates the lower boundary for acceptable phase velocities, but not the higher ones (plateau, see Figure 14, bottom left). The frequency, from which phase differences cannot be resolved any more, depends on the maximum inter-station distance and the S-wave velocity structure below the site: a wide range of velocities will then explain the observed small phase differences. Zhang et al. (2004) clearly pointed out this problem in Equation (3a) of their article.

Figure 15 shows the final dispersion curve.

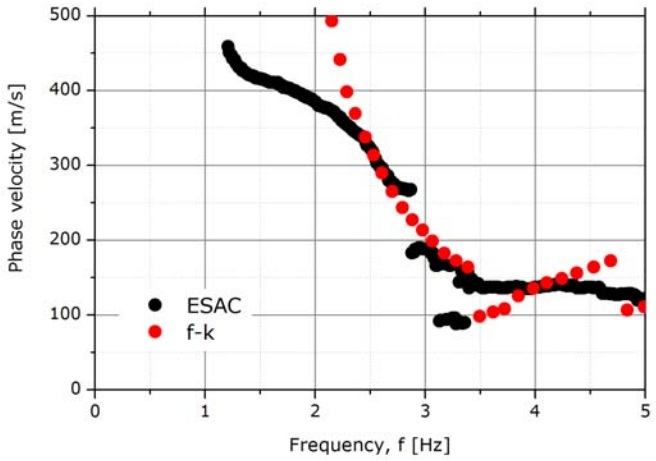

Figure 15 – Phase velocity dispersion curves obtained by ESAC, and f-k analysis at the Bevagna test site.

3.2.2 Interferometry and tomography

Recent theoretical studies have shown that the cross-correlation of diffuse wavefields can provide an estimate of the Green's functions between receivers (Weaver & Lobkis 2001, 2004; Snieder 2004; Wapenaar 2004; Wapenaar & Fokkema 2006). Using coda waves of seismic events (Campillo & Paul 2003) and long seismic noise sequences (Shapiro & Campillo 2004), it was confirmed that it is possible to estimate the Rayleigh wave component of Green's functions between two stations by the cross-correlation of simultaneous recordings, a method now generally referred to as seismic interferometry. These results allowed the first attempts of surface wave tomography at regional scales (e.g. Shapiro&Campillo 2004; Sabra *et al.* 2005; Shapiro *et al.* 2005; Gerstoft *et al.* 2006; Yao *et al.* 2006; Cho *et al.* 2007; Lin *et al.* 2007; Yang *et al.* 2007) using seismic noise recordings from broad-band seismic networks. Generally, for these kinds of studies, waves at frequencies well below 1 Hz were used to image the crust and the upper-mantle structure. A comprehensive review of the seismic interferometry method can be found in Curtis *et al.* (2006).

Seismic noise interferometry can be also applied to frequencies greater than 1Hz. Schuster (2001) and Schuster *et al.* (2004) demonstrated the possibility of forming an image of the subsurface using the cross-correlation of seismic responses from natural and man-made sources at the surface or in the subsurface. Furthermore within the context of exploration geophysics, Bakulin & Calvert (2004, 2006) first proposed a practical application of seismic interferometry, showing that it is possible in practice to create a virtual source at a subsurface receiver location in a well. Other recent applications for the high-frequency range have been proposed by Dong *et al.* (2006) and Halliday *et al.* (2007) for surface wave isolation and removal in active-source surveys. Among the several reasons that have stimulated the application of seismic noise interferometry to high frequencies, there is the possibility of applying this technique to suburban settings (Halliday *et al.* 2008), and then to exploit this approach for engineering seismology purposes. Such an application requires knowledge of the subsurface structure from depths of a few metres to several hundred of metres, and for this reason interest has moved towards the high-frequency range.

The application of seismic noise interferometry to high frequencies is not a merely change of scale, since it involves important questions still under discussion within the research community. For example, the effects of the high spatial and temporal variability in the distribution of noise sources occurring at high frequencies are still under investigation

(Halliday & Curtis 2008a,b), as well as the relationship between the wavelength of interest and station interdistances. Several authors (e.g. Chavez-Garcia & Luzon 2005; Chavez-Garcia & Rodriguez 2007; Yokoi & Margaryan 2008) showed, for a small scale experiment at a site with a homogeneous subsoil structure, the equivalence between the results obtained by crosscorrelation in the time domain and the SPatial Auto-Correlation analysis (SPAC) method (Aki 1957). However, it is worth noting that for non-homogeneous subsoil conditions, the SPAC method suffers a severe drawback. That is, generally, such a method is used to retrieve the shallow soil structure below a small array of sensors by means of the inversion of surface wave dispersion curves extracted by seismic noise analysis. In particular, the inversion is performed under the assumption that the structure below the site is nearly 1-D. Therefore, if the situation is more complicated (2-D or 3-D structure), then the SPAC method can only provide a biased estimate of the *S*-wave velocity structure. On the contrary, one can expect that, similarly to what is obtained over regional scales, local heterogeneities will affect the noise propagation between sensors, and hence can be retrieved by analysing the Green's function estimated by the cross-correlation of the signals recorded at two different stations. For this reason, passive seismic interferometry is also believed to be a valuable tool for studying complex structure and estimating surface wave tomography also for smaller spatial scales of investigation. Just recently, Picozzi et al. (2008) verified the suitability of seismic interferometry for seismic engineering and microzonation purposes. In fact, after having first evaluated the possibility of retrieving reliable and stable Green's functions within the limitations of time and instrumentation that bound standard engineering seismological experiments (for example, in urban microzonation studies, the number of deployed sensors is generally not larger than 20 and the acquisition time does not last more than a few hours) they applied the seismic interferometry technique to recordings from a 21-station array installed in the Nauen test site (Germany) (http://www.geophysik.tuberlin. de/menue/testfeld_nauen/; Yaramanci *et al.* 2002). They showed that passive seismic interferometry is a valuable tool for the characterization of near-surface geology since the travel times estimated from the Green's functions analysis for different frequencies were inverted to derive, innovatively due to the frequency range investigated and the scale of the experiment, the laterally varying 3-D surface wave velocity structure below the array.

Figure 16 shows a 2D cross section highlighting lateral velocity variations as inferred by seismic tomography from the application of seismic interferometry to seismic noise (Picozzi et al., 2008).

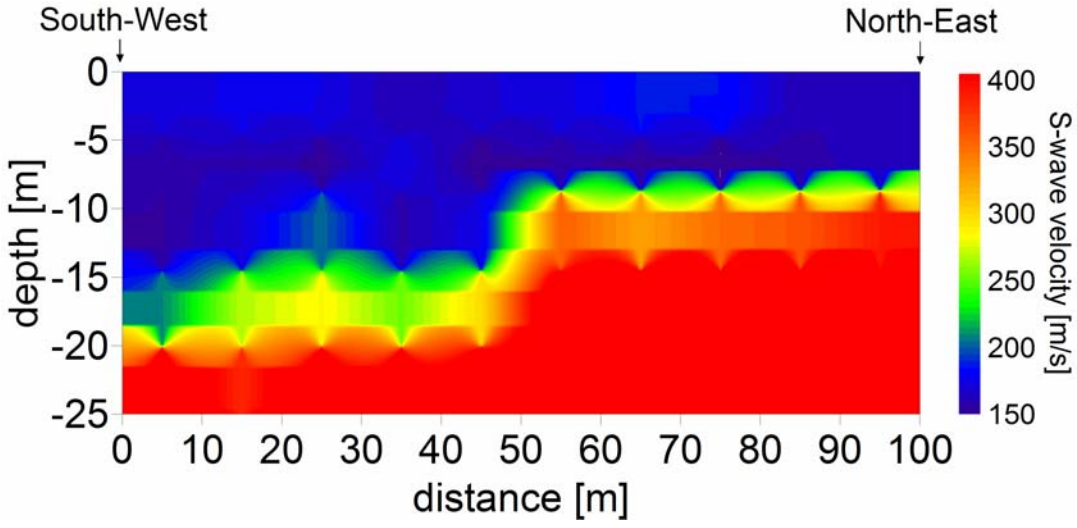

Figure 16 – S-wave velocity section extending southwest to northeast in the centre of the study area of Picozzi et al., 2008, derived by sismic noise tomography.

3.3 Seismic Noise Horizontal-to-Vertical spectral ratio NHV

In 1989 Nakamura (Nakamura, 1989) revised the Horizontal-to-Vertical (H/V) spectral ratio of seismic noise technique, first proposed by Nogoshi and Igarashi (1970, 1971). Since then, in the field of site effect estimation, a large number of studies using this low cost, fast and therefore, attractive, technique have been published (e.g. Field and Jacob, 1993; Lermo and Chavez-Garcia, 1994; Mucciarelli, 1998; Bard, 1998; Parolai et al., 2001). Most of the researchers focused their attention on the comparison of noise H/V spectral ratio and earthquake site response and agreed that the H/V spectral ratio of seismic noise provides a fair estimate of the fundamental resonance frequency of a site. However, attempts to provide standards for the analysis of seismic noise have only recently been carried out (Bard, 1998; SESAME, 2003; Picozzi et al., 2005).

3.3.1 NHV peak-thickness of the sedimentary cover relationships

Recent studies (Yamanaka et al., 1994; Ibs-von Seht and Wohlenberg, 1999; Delgado et al., 2000 a, b, Parolai et al., 2001, D'Amico et al., 2008) showed that noise measurements can be used to map the thickness of soft sediments. Quantitative relationships between this thickness and the fundamental resonance frequency of the sedimentary cover, as determined from the peak in the NHV spectral ratio were calculated for different basins in Europe (e.g. Ibs-von Seht and Wohlenberg, 1999; Delgado et al., 2000 a).

The approach is based on the assumption that in the investigated area, lateral variations of the S-wave velocity are minor and that it mainly increases with depth following a relation like

$$v_s(z) = v_{s0}(1+Z)^x \tag{22}$$

where v_{s0} is the surface shear wave velocity, $Z=z/z_0$ (with z_0=1 m) and x describes the depth dependence of velocity. Taking this into account and considering the well known relation among f_r (the resonance frequency), the average S-wave velocity of soft sediments $\overline{V_s}$, and its thickness h,

$$f_r = \overline{V_s} / 4h \tag{23}$$

The dependency between thickness and f_r thus becomes

$$h = \left[v_{s0} \frac{(1-x)}{4 f_r} + 1 \right]^{1/(1-x)} \tag{24}$$

where f_r is to be given in Hz, v_{s0} in m/sec and h in m.

Moreover, empirical relationships between f_r and h in the form

$$h = a f_r^{\,b} \tag{25}$$

can also be derived, generally applying grid search procedures.

The above approximate interpretation can be easily extended to the case of two layer sedimentary cover (D'Amico et al., 2008). Despite of the fact that relatively large errors affect the depth estimates provided by this approach (D'Amico et al., 2004) it can be considered as a useful proxy for exploratory purposes.

3.3.2 NHV inversion

Recently, the possibility of retrieving the S-wave velocity structure below a site from single station measurements based on NHV ratio computation was tested by Fäh et al. (2001). They suggested a new method for calculating NHV ratios employing a time-frequency analysis (FTAN). Moreover, after having shown that there is a good agreement between the NHV ratio and the theoretical ellipticity curves of the fundamental mode Rayleigh wave, they proposed to invert the NHV curve to derive directly the S-wave subsoil structure. The NHV was corrected for the contamination by SH and Love waves by simply reducing it by a factor $\sqrt{2}$, independent of frequency. The inversion, due to the non-linear nature of the problem, was based on a genetic algorithm (GA) (Fäh et al., 2001, 2003). The inversion is carried out for a fixed number of layers and a-priori defined ranges of the geophysical properties (S-wave, P-wave, density and thickness) of the layers. An initial starting population of individuals is generated through a uniform distribution in the parameter space. The model that, amongst all those generated, allows the best reproduction of the observed NHV, is chosen as the best model.

Figure 17 shows the S-wave velocity profiles obtained by inverting NHV curves (calculated in a standard way and by FTAN) for a site in the Cologne area (Parolai et al., 2006).

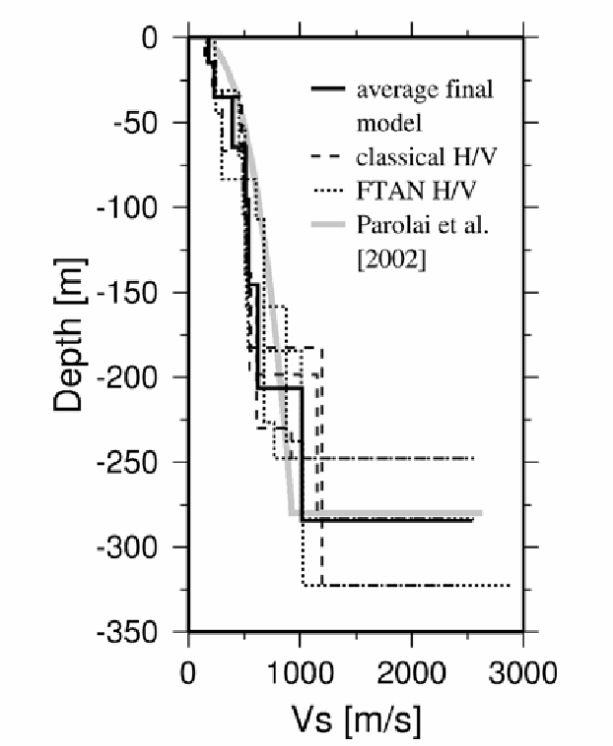

Figure 17 – NHV ratio inversion results for the Pulheim site (Cologne). For both the classical and the FTAN methods, results from fixing different sedimentary cover thicknesses (thin/thick sediments) are shown (from Parolai et al., 2006).

The inversion was carried out by fixing the total thickness of the sedimentary cover in order to avoid problems of trade-off between the total thickness and the S-wave velocity (Scherbaum et al., 2003; Arai and Tokimatsu, 2004). Three different values for the total thickness of the sediments were considered: the average value from an empirical relation between velocity versus depth calculated for the investigated area and the maximum and minimum values considering the standard errors in that relationship. Figure 18 shows the fit to the average NHV ratios.

Finally, the derived S-wave velocity profiles have been compared with those obtained by array techniques (Parolai et al., 2006) and an excellent agreement was found.

In Parolai et al., (2006) the inversion of NHV curves was extended to 20 of the sites measured by Parolai et al. (2001) and a 2D S-wave velocity model was derived by means of interpolating between the derived 20 profiles. Figure 19 shows the resulting 2D S-wave velocity model (bottom) together with the geological cross-section. The agreement between the geological structure and the S-wave velocity model is obviously very good. Compared to the average velocity relationship previously derived for the whole area, lateral variations in the velocity structure are clearly visible.

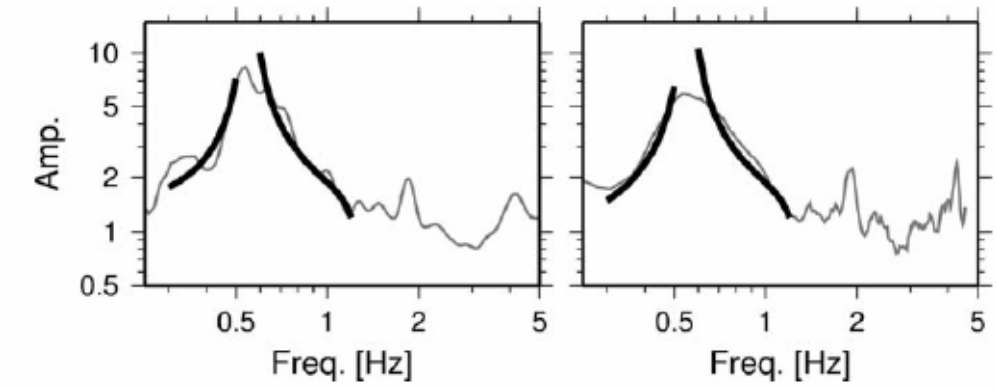

Figure 18 – Example of average NHV ratios inverted in Cologne: classical analysis (left) and FTAN method (right). The fundamental mode Rayleigh wave ellipticity calculated for one of the final GA models is indicated in black. (from Parolai et al., 2006)

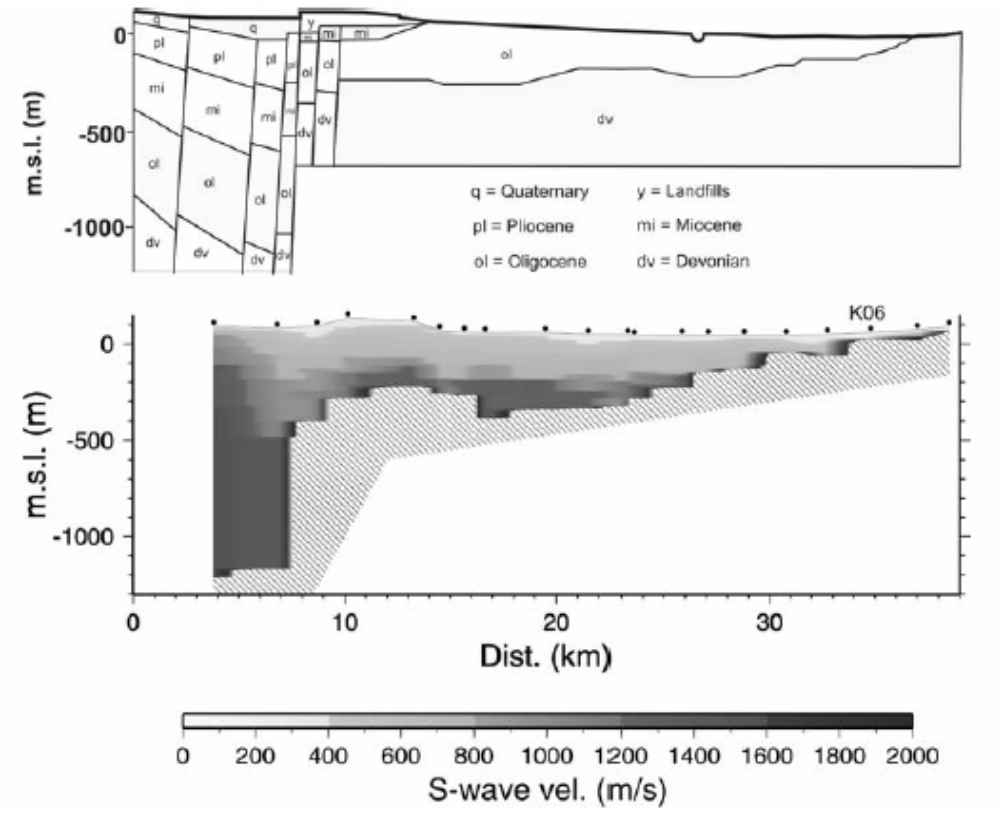

Figure 19 – Top: Geological cross section of the sedimentary cover in Cologne. Bottom: 2D S-wave velocity model interpolated from 1D S-wave velocity profiles calculated for the 20 selected sites (Parolai et al., 2006). The striped pattern indicates the Devonian bedrock.

Therefore, it was shown that given that the bedrock depth can be constrained and the sedimentary cover is fairly regularly layered, the NHV inversion is a suitable method for quickly mappping 3D S-wave velocity structures. The vertical resolution of the profiles was also found sufficient to provide site responses (Parolai et al., 2006; Parolai et al., 2007) by means of numerical simulations, in agreement with the empirical ones.

More recently, improvement in the forward calculation of NHV spectral ratios were proposed by Arai and Tokimatsu (2000, 2004) and applied in a joint inversion scheme of NHV and dispersion curves by Parolai et al. (2005), Picozzi and Albarello (2007), D'Amico et al. (2008).

Arai and Tokimatsu (2000) showed that NHV spectral ratios can be better reproduced if the contribution of higher modes of Rayleigh waves and Love waves is also taken into account. They suggest to calculate the NHV spectral ratio as :

$$\left(\mathrm{NHV}\right)_s = (P_{HS}/P_{VS})^{1/2} \tag{26}$$

where the subindex s stands for surface waves, and P_{VS} and P_{HS} are the vertical and horizontal powers of surface waves (Rayleigh and Love), respectively.

The vertical power of the surface waves is only determined by the vertical power of Rayleigh waves (P_{Vr}), while the horizontal power must consider the contribution of both Rayleigh (P_{Hr}) and Love waves (P_{HL}). The following equations can therefore be used:

$$P_{VS} = P_{VR} = \sum_j \left(A_{Rj}/k_{Rj}\right)^2 \left\{1 + \left(\alpha^2/2\right)\left(u/w\right)_j^2\right\} \tag{27}$$

$$P_{HS} = P_{HR} + P_{HL} \tag{28}$$

$$P_{HR} = \sum_j \left(A_{Rj}/k_{Rj}\right)^2 \left(u/w\right)_j^2 \left\{1 + \left(\alpha^2/2\right)\left(u/w\right)_j^2\right\} \tag{29}$$

$$P_{HL} = \sum_j \left(A_{Lj}/k_{Lj}\right)^2 \left(\alpha^2/2\right) \tag{30}$$

where A is the medium response, k is the wavenumber, u/w is the H/V ratio of the Rayleigh mode at the free surface, j is the mode index, and α is the H/V ratio of the loading horizontal and vertical forces L_H/L_V. Parolai et al. (2005) showed that varying α over a large range did not significantly changed the NHV shape. Therefore, they used $\alpha=1$.

A basic problem of these inversion procedures is choice of frequency band to be considered for the inversion of the NHV curve. As an example, the NHV values around the maximum (see Fig. 18) have been discarded by Parolai et al. (2006) and instead taken into account by Picozzi and Albarello (2007) and D'Amico et al. (2008). Recent theoretical studies (Lunedei and Albarello, 2009; Albarello and Lunedei, 2009) indicated that NHV curve around the fundamental resonance frequency f_0 (i.e., around the NHV maximum) can be significantly affected by the damping profile in the subsoil and by the distribution of sources around the receiver. In particular, they showed that sources located within few hundreds of meters from the receiver can generate seismic phases that strongly affect the shape of the NHV curve around and below f_0. This implies that, unless a large source-free area exists around the receiver, inversion of the NHV shape (around and below $f_{0)}$ carried out using forward models based on surface waves only, might provide biased results,

4. Inversion methods

4.1 The Forward modelling

The basic element of the inversion procedure is the availability of a fast and reliable tool for solving the forward problem. Theoretical modelling suggests that the dispersion curves of the fundamental and higher mode Rayleigh waves and the NHV spectral ratio mainly depend non-linearly on the S-wave velocity structure, but also the density and P-wave velocity structure. As concerns the damping profile, the sensitivity of the Rayleigh and Love waves dispersion curve results relatively weak while much more sensitive to this parameter appears to be the NHV curve (Lunedei and Albarello, 2009).

Several procedures exist to compute expected surface waves amplitudes and propagation velocity (both for the fundamental and higher modes) in the case of a flat weakly or strongly dissipative layered Earth (e.g., Buchen & Ben-Hador 1996; Lai and Rix, 2002). In general, modal characteristics of surface waves are provided in implicit form (zeroes of the normal equation) and this implies that numerical aspects play a major (see e.g., Lai and Wilmanski, 2005). Thus, the effectiveness of available numerical protocols (e.g., Herrmann, 1987) mainly relies on their capability in reducing numerical instabilities (mode jumping, etc.).

In order to simplify the problem, the dominance of fundamental propagation mode is commonly assumed. However, several studies (e.g. Tokimatsu et al., 1992; Foti, 2000; Zhang and Chan, 2003, Parolai et al., 2006) showed that for sites with S-wave velocities varying irregularly with depth (low velocity layers embedded between high velocity ones) a higher mode or even multiple modes dominate certain frequency ranges. This results in an inversely dispersive trend in these frequency ranges. Therefore, due to the contribution of higher modes of Rayleigh waves, the obtained phase velocity has to be considered an apparent one. Moreover, other studies (Karray and Lefebvre, 2000) showed that even at sites with S-wave velocity increasing with depth, the fundamental mode does not dominate always. Tokimatsu et al. (1992) formulated the apparent phase velocity derived from noise-array data as the superposition of multiple-mode Rayleigh waves. Ohori et al. (2002) adopted this formulation making use of the method of Hisada (1994) for calculating the dispersion curves. Assuming that source and receivers are located only at the surface, Tokimatsu et al. (1992) proposed that the apparent phase velocity is related to the multiple-mode Rayleigh waves through:

$$c_{si}(f) = 2\pi f r \left\{ \cos^{-1} \left[\frac{\sum_{m=0}^{M} A_m^2(f) c_m(f) \cos\left(\frac{2\pi f r}{c_m(f)} \right)}{\sum_{m=0}^{M} A_m^2(f) c_m(f)} \right] \right\}^{-1}, \qquad (31)$$

where $c_{si}(f)$ is the apparent phase velocity, $c_m(f)$ and $A_m(f)$ are the phase velocities of the mth mode Rayleigh wave and the corresponding medium response (Harkrider, 1964). $A_m(f)$ is related to the power spectrum density function of the mth mode, M is the maximum order of mode for each frequency, and r is the shortest distance between sensors. Parolai et al, (2006) confirmed that in the case of subsoil profiles with low velocity layers leading to apparent dispersion curves, the inversion carried out only considering fundamental modes yield to artifacts in the derived S-wave velocity profiles.

The presence of upper modes is also responsible for a further problem. The number of existing modes depends on the frequency (Aki and Richards, 1980): this implies that, depending on the subsoil configuration, abrupt changes exist in this number as a function of frequency (modal truncation). When upper modes play a significant role, their sudden

disappearance results in unrealistic jumps in the computed dispersion and NHV curves. To reduce this problem, a number of fictitious very thick layers (of the order of Km) has to be added below the model to prevent artefacts. Of course, the parameters of these layers cannot be resolved by experimental curves and have the only role to prevent modal truncation effects.

Beyond these problems, one should be aware that surface waves only represent a part of the existing wave field. Other seismic phases (near field, body waves) also exist and could play a major role. This problem could be easily faced in active survey, by selecting suitable source-receiver distances. However, when passive procedures are of concern, it is not possible to select suitable sources and some problems could arise. In general, seismic array procedures (fk, ESAC, SPAC) allow to individuate and remove the effect of such waves. However, this cannot be done in single station setting (NHV). These effect have been explored theoretically (Albarello and Lunedei, 2009) by modelling the average complete noise wave field generated by surface point sources. This study revealed that the surface waves solution only holds (above the fundamental resonance frequency) in the case that a source free area of the order of several tens to hundreds meters (depending on the subsoil configuration) exists around the receiver.

A basic problem of the forward modelling concerns the possible presence of lateral heterogeneities in the subsoil structure. In general, such lateral variations dramatically affect both amplitudes and propagation velocities. However, it can be shown (e.g., Snieder, 2002) that when the wavelength of concern is much larger than the horizontal scale length of structural variation, *local modes* can be considered. These are defined at each horizontal location (x, y) as the modes that the system would have if the medium would be laterally homogeneous. That is, the properties of the medium at that particular location (x, y) can be considered to be extended laterally infinitively.. In this approximation, 1D models can be applied making also possible the development of approximate surface waves tomographic approaches (Picozzi et al., 2008).

4.2 Inversion procedures

Hence, the final model calculated by a linearized inversion inherently depends on an assumed initial model because of the existence of local optimal solutions. When an appropriate initial model may be generated using a-priori information about the subsurface structure, linearized inversions can find an optimal solution that is the global minimum of a misfit function. Other methods can be used to solve the non-linear problem either using local search methods or global search methods. In this respect, a wide variety of techniques have been proposed, among which the following are commented: the simplex downhill method (Nelder and Mead, 1965), the Monte Carlo approach and the genetic algorithm (e.g. Goldberg, 1989). In contrast to linearized inversions schemes, the non-linear inversion schemes require only an evaluation of the functions, not their derivatives.

Linearized Inversion (LIN; for more information see Tokimatsu et al., 1991, and Xia et al., 1999, Arai and Tokimatsu,2005)

The inverse problem is generally solved using Singular Value Decomposition (SDV, Press et al., 1986) and the RMS of differences between observed and theoretical phase velocities (or in case of NVV between observed and theoretical NHV) are minimized. Because of the non-linearity of the problem the inversion is repeated until the RMS ceases to change significantly. Also, iterative inversion techniques like the simultaneous iterative reconstruction technique (Van der Sluis and Van der Vorst, 1987) are used, but they do not provide any advantage with respect to using SVD. Importantly, LIN heavily relies on a good starting model.

Simplex Downhill Method (SDM; Nelder and Mead, 1965, Parolai et al., 2006)

Ohori et al. (2002) proposed to use this method to minimize the discrepancy between the squared differences of observed and theoretical phase velocities, normalized to the squared value of the observed velocities. For multi-dimensional minimizations, the algorithm requires an initial estimate. Generally, two chosen starting points are provided. The solution with the minimum misfit is adopted and the inversion then repeated, restarting from this solution. The SDM quickly and easily locates a minimum, hereby however it might miss the global one eventually.

MonteCarlo Method (MC; Press, 1968, Socco and Boiero, 2008)

In Monte Carlo (MC) procedures (Tarantola, 2005) the space of model parameters is randomly explored and the numerical dispersion curves associated to each of several possible shear wave velocity profiles is compared to the experimental dispersion curve. One of the main problems is the need of exploring a sufficient number of profiles in order an adequate sampling of the model parameters space. An efficient inversion algorithm for the inversion of surface wave data makes use of the scale properties of the dispersion curves (Socco and Boiero, 2008). These properties are linked to the scaling of the modal solution with the wavelength. If model parameters are scaled, the corresponding modal dispersion curve scales accordingly: in particular both phase velocities and frequencies scale if all the layer velocities are scaled, while only the frequencies scale if all the layer thicknesses are scaled (Socco and Strobbia, 2004).

Modified Genetic Algorithm (GA; Yamanaka and Ishida, 1996; Parolai et al., 2005)

With this algorithm, a search area is defined both for the S-wave velocity and thickness of the layers. An initial population of a limited number of individuals (e.g. 30) is generated and genetic operations are applied in order to generate a new population with the same size. This new population is reproduced based on a fitness function for each individual. In this study, the fitness function was defined considering the average of the differences between the observed and the theoretical phase velocities. In addition to the crossover and mutation operation, two more genetic operations were used to increase convergence, namely elite selection and dynamic mutation. Elite selection assures that the best model appears in the next generation, replacing the worst model in the current one. To avoid a premature convergence of the solution into a local minimum, the dynamic mutation operation was used to increase the variety in the population. Therefore, GA is a non-linear optimization method that simultaneously searches locally and globally for optimal solutions by using several models.

Since this inversion applies a probabilistic approach using random numbers and finds models near to the global optimal solution, it is repeated several times by varying the initial random number. The optimal model is selected considering the minimum of the chosen fitness function. Recently Picozzi and Albarello (2007) suggested to combine the GA inversion with a linearised one. In practice the linearised inversion is started using as input model the best model of the GA inversion that it is supposed to be located close to the global minimum solution.

5. Case histories

5.1 Microtremor measurements interpretation at the BVG station of Italian accelerometric Network (Rete Accelerometrica Italiana, RAN)

Microtremor measurements in array configuration were carried out by INGV-Mi in September 2007 at a test site in Bevagna (Italy) near the BVG station of the Italian Accelerometric Network (Figure 20). The BVG station was installed on a clayey formation (fluvial sediments in Figure 20b-c) which may influence earthquake records in the frequency band of engineering interest. The purpose of this study is the characterization of the clayey formation under the BVG station in terms of shear wave velocity (V_S), i.e. the most representative parameter to estimate the subsoil seismic response.

Data were recorded for more than 3 hours through 15 LE-3D/5s sensors connected to a Reftek 130 digitizer and the sampling rate was fixed to 500 Hz, that is adequate for the frequency range and the inter-station distance considered. Supposing significant lateral V_S variations not affect the volume under the array measurement, observed Rayleigh and Love wave dispersion characteristics were reproduced through two different inversion methods. In both analyses Horizontal-to-Vertical Spectral Ratios of ambient vibrations (NHV) were used as a threshold for low frequencies, allowing to extend the depth of investigation.

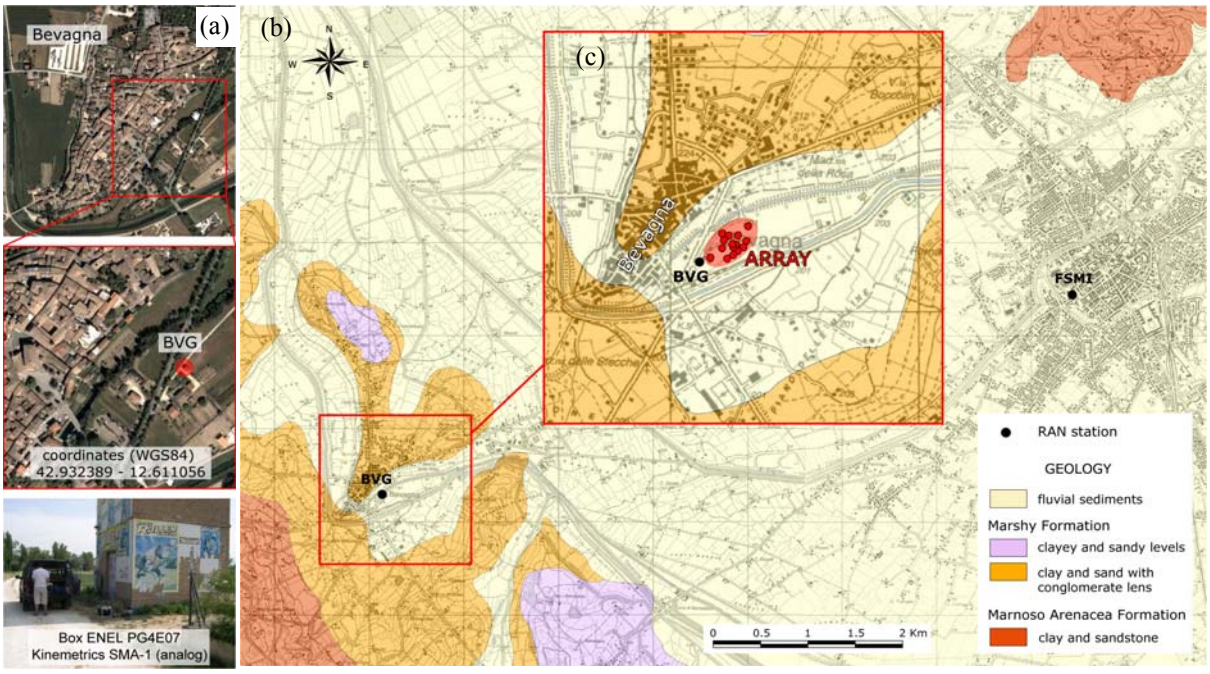

Figure 20 − Location of the Italian Accelerometric Network BVG station (a): geology settings of the study area (b); and relative position of BVG station and array measurements (c).

Rayleigh wave dispersion curve analysis

Experimental Rayleigh-wave dispersion curves were estimated both by the f-k analysis (cf. §3.2.1) and the ESAC method (cf. §3.2.2) using some Fortran and Matlab routines. Synchronized microtremor records were selected from the vertical component of each station to compute the two dispersion curves for Rayleigh waves: about 50 signal windows of 60 seconds were used (50 for f-k analysis and 46 for ESAC method).

The ESAC Rayleigh-wave dispersion curve was obtained minimizing the root mean square (RMS) of the differences between the experimental and the theoretical Bessel function values (Figure 21). On the basis of estimated phase velocity at each frequency, only the recordings at distance less than 1.5 times of the relevant wavelength were considered. This limit was applied to reduce the bias in the phase velocity estimation due to anthropic noise around 3 Hz (cf. f-k analysis results in the next pages).

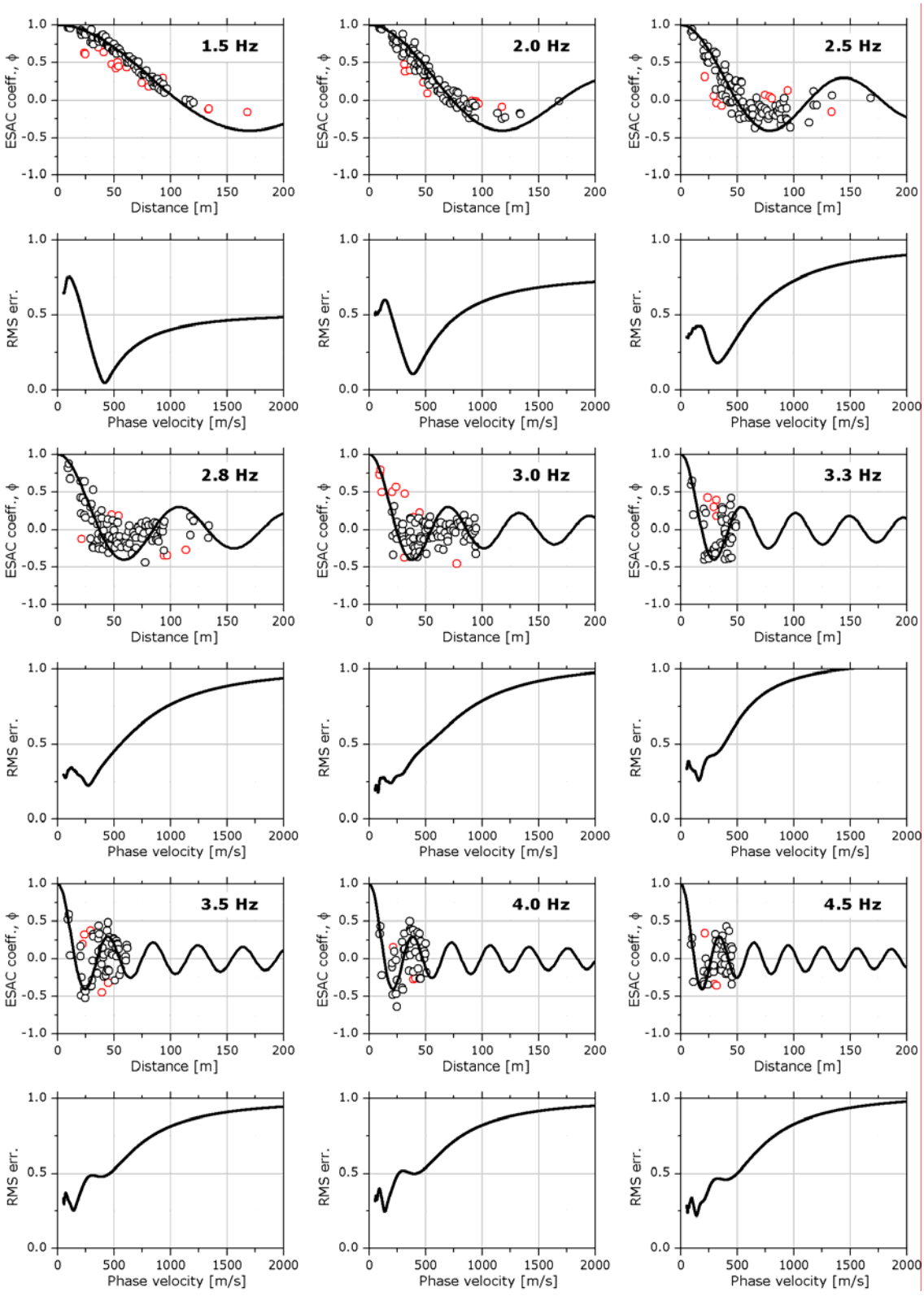

Figure 21 – ESAC: Experimental space-correlation function values (circles) for different frequencies. The red circles indicate values discarded. The black lines depict the estimated space-correlation function values for the phase velocity showing the best fit to the data and the relevant RMS error versus phase velocity curves.

Figure 22 shows the good agreement between the Rayleigh wave dispersion curves estimated both with ESAC and f-k approaches (Maximum Likelihood Method). Only below 2.5 Hz the f-k analysis provide larger phase velocities. The disagreement toward the lower frequencies confirms the results of previous studies (Parolai et al., 2007). Furthermore, problems arise with the ESAC method in estimating the phase velocity at around 3 Hz due to a strong persistent and directional source of noise.

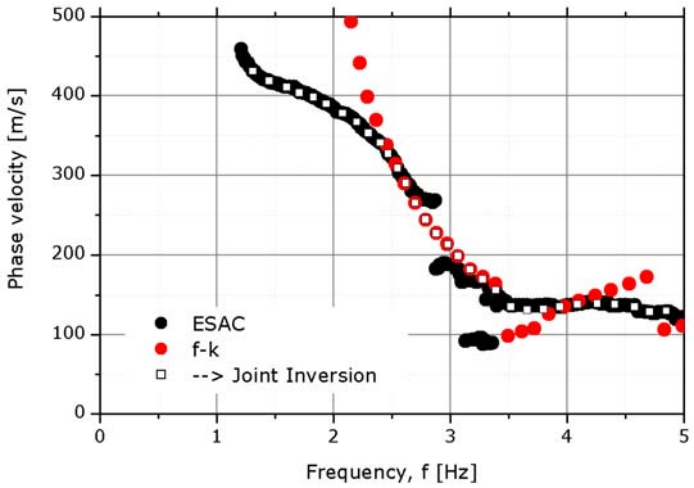

Figure 22 – Comparison of experimental phase velocity estimated by the ESAC method and by the f-k method. The white squares represent the values used to joint inversion.

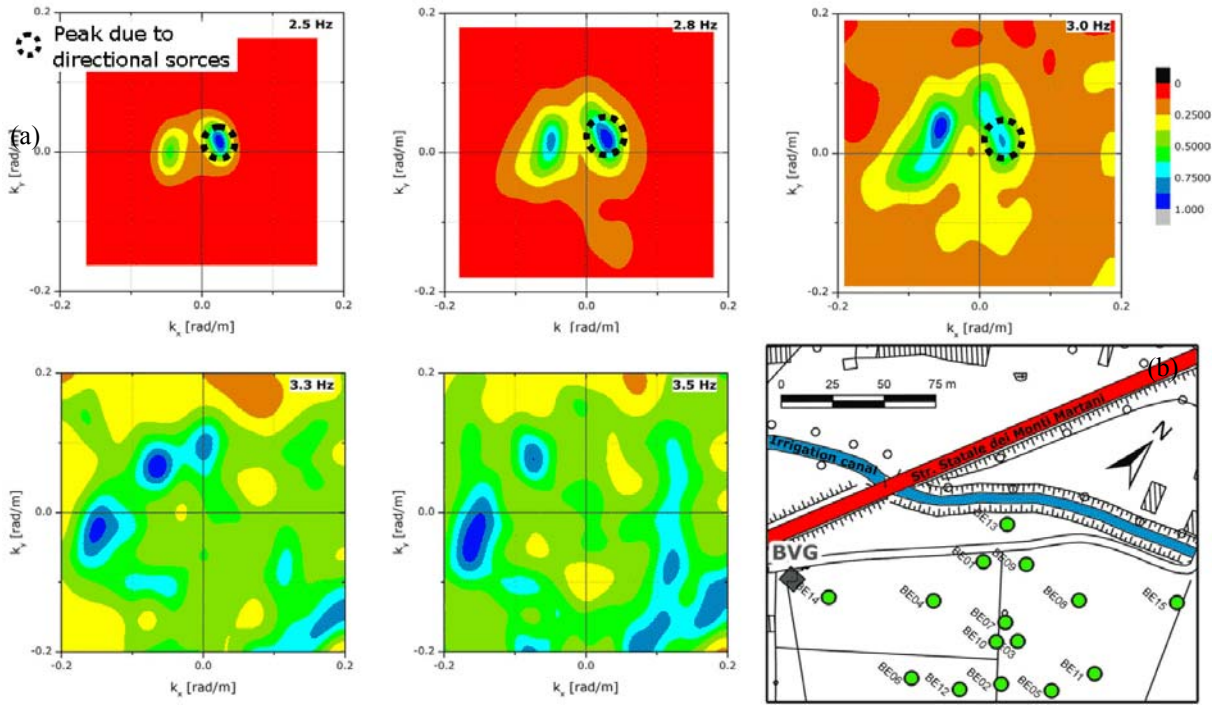

Figure 23 – F-k power density function at different frequencies (a) and map of the array measurement with the respective position of the "Statale dei Monti Martani" street and of an irrigation channel (b).

The f-k analysis offers the opportunity to verify if the requirements on the noise source distribution for the application of the ESAC analysis were fulfilled and, overall, the reason of the poor coherency of the ESAC curve around 3 Hz. Figure 23 shows the output of the frequency-wavenumber analysis at various frequencies.

In Figure 23a contour plots at 2.5, 2.8 and 3.0 indicate the presence of noise propagating from two different directions. In particular, they evidenced that the highest energy is propagating from northeast (cf. map in Figure 23b) with a velocity of about 500 m/s. This velocity is estimated applying equation (13) in correspondence of the f-k power density functions peaks (cf. contour maps in Figure 23 and the relevant values reported in Figure 24 with green circles and in Table 1). The high peaks with high velocity of propagation which appear on contour plots of f-k power density function between 2.5 and 3 Hz may be probably due to human activities, but a clear location of the source was not yet possible. However, the activities existing in the nearby irrigation channel (evidenced by a blue colour in the map in Figure 23) could explain this source of noise.

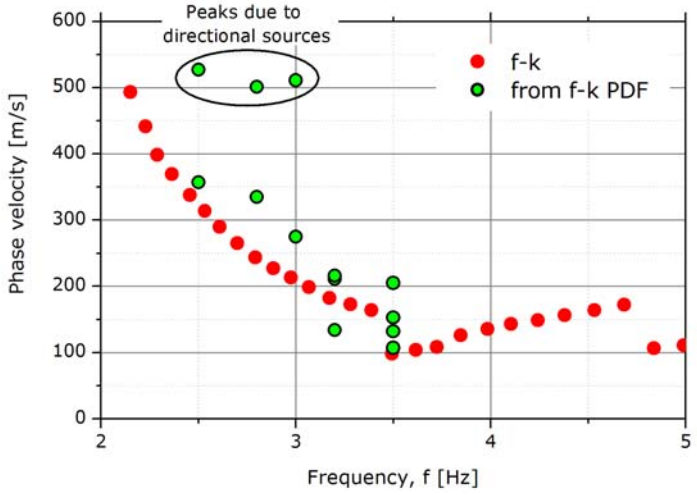

Figure 24 – Observed Rayleigh-wave dispersion curves estimated by the ESAC method and by the f-k method. Green circles represent the phase velocity directly obtained from f-k power density functions through equation (13).

f_0	k_{x0}	k_{y0}	c_0
2.5	*0.0247*	*0.0166*	*527*
	-0.0439	0.0008	357
2.8	*0.0294*	*0.0193*	*501*
	-0.0499	0.0161	335
3.0	*0.0314*	*0.0193*	*511*
	-0.0541	0.0422	275
3.2	0.0001	0.0954	211
	-0.0656	0.0663	216
	-0.1480	-0.0214	134
3.5	-0.0739	0.0777	205
	-0.1605	-0.0422	132
	0.0835	-0.1873	107
	0.1200	-0.0798	153

Table 1 – Phase velocity directly obtained from f-k power density functions peaks.

Considering the observed reliability of the two methods (ESAC and f-k) in estimating the phase velocity in different frequency bands for the data set at hand, we decided to combine the ESAC dispersion curve in the range 1.3÷2.5 Hz and 3.5÷5 Hz with the f-k dispersion curve in the 2.5÷3.5 Hz range. The obtained dispersion curve is then considered in the inversion (Figure 22).

On the other hand, also NHV was used to constrain inversion. Smoothed NHV were calculated according to equation:

$$\frac{H}{V} = \frac{\sqrt{NS^2 + WE^2}}{UP} \tag{32}$$

For each station, 50 signal windows of 200 s were used and the relevant spectral ratio amplitudes – calculated by equation (32) – were considered log-normally distributed to estimate the average curve.

A predominant frequency of 1.0 Hz appear at all stations (Figure 25), except for BE01, BE09 and BE13. Being these stations on the external boundary of the array, their different

frequency response could be associated to lateral variations and/or close noise sources (cf. map in Figure 23). For this reason, microtremors recorded at BE01, BE09 and BE13 stations were not considered to construct the mean NHV. Although LE-3D/5s sensors can reproduce frequencies in the range 0.2÷40 Hz (cf. technical data sheet at www.lennartz-electronic.de), the minimum reliable frequency here considered is 0.5 Hz, since the trend of NHV ratios at lower frequencies clear shows problems due to installation (BE02, BE05, BE06, BE08, BE11, BE12 and BE15).

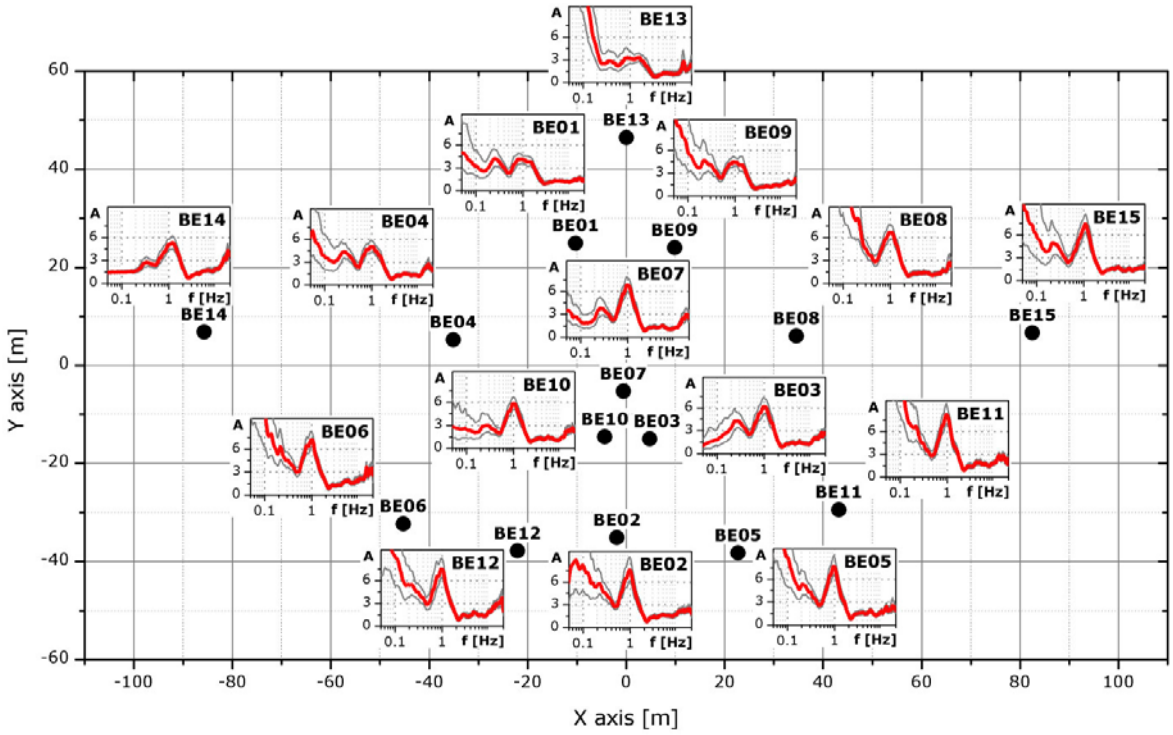

Figure 25 – NHV of the array microtremor measurements.

The joint inversion of dispersion and NHV curves was carried out using a geotechnical model which consist in 7 horizontal layers overlying an half-space (Table 2). Through a genetic algorithm a search over 80000 models was carried out and the theoretical NHV and Rayleigh-wave dispersion curve were compared with the empirical ones. Higher modes (higher modes can be excited in seismic noise especially if velocity inversions are present) were considered while calculating NHV and dispersion curves.

	Shear wave velocity, V_S [m/s]		Thickness, h [m]		Density, ρ [ton/m^3]
Layer	MIN	MAX	MIN	MAX	
#1	70	200	10	20	1.8
#2	70	250	5	10	1.9
#3	150	400	10	30	1.9
#4	200	500	10	50	2.0
#5	250	650	15	50	2.1
#6	350	800	20	100	2.2
#7	450	1100	50	350	2.2
Half-space	600	2500	Infinite		2.3

Table 2 – Parameters ranges used to join inversion.

The genetic algorithm allows to vary the thickness and the shear wave velocity for each layer. On the contrary, for each layer, density was assigned *a priori*, while compression wave velocity (V_P) were calculated after defining the values of the shear wave velocity (V_S) via the equation:

$$V_P\,[\mathrm{m/s}] \;=\; 1.1 \cdot V_S + 1290 \tag{33}$$

proposed and validated for deep soil deposits by Kitsunezaki et al. (1990). Poisson's ratio was then obtained as a function of V_S and V_P. The inversion is repeated starting from different seed numbers that determine a different initial population of models. In this way it is possible to better explore the space of the solution.

The models are selected on the basis of a cost function considering empirical and computed NHV (*hv*) and Rayleigh-wave dispersion (*c*) curves (defined after Herrmann et al., 1999):

$$\mathrm{cost} = \left[(1-p)N + pK\right] \cdot \left\{ \frac{1-p}{N} \left[\sum_{j=1}^{N} \left(\frac{c_O(f) - c(f)}{c_O(f)} \right)^2 \right] + \frac{p}{K} \left[\sum_{j=1}^{K} \left(\frac{hv_O(f) - hv(f)}{hv_O(f)} \right)^2 \right] \right\} \tag{34}$$

where the subscript *o* indicates observed data, while *N* and *K* are the number of data points in the dispersion and NHV curves, respectively. The relevant influence of both data sets is controlled by the parameter *p*. If *p*=0 the inversion is performed using only the apparent dispersion curve, while the inversion relies exclusively on the NHV for *p*=1. In this application, we chose after trial and error test the weight *p*=0.04. Best models are selected minimizing this cost function (Figure 26d).

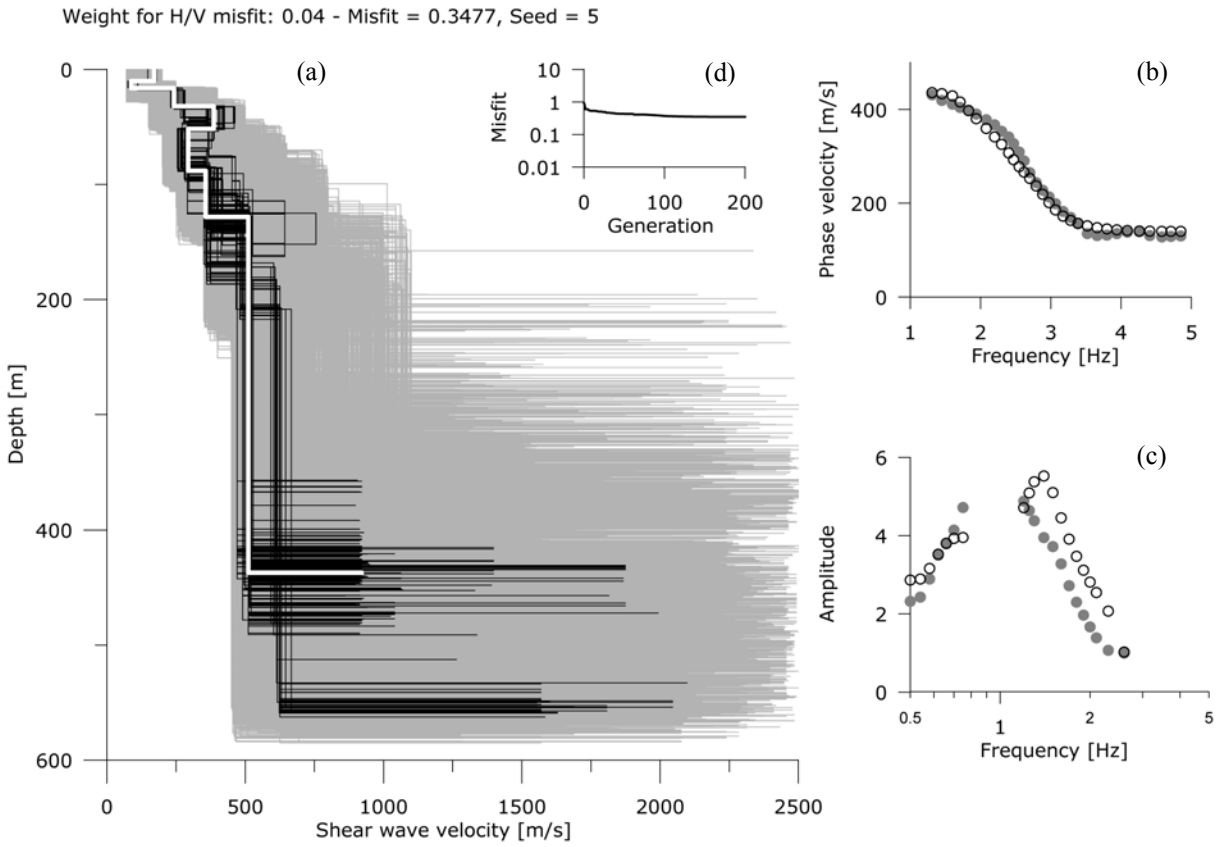

Figure 26 – Subsoil model at the BVG station (a) and its fit to the dispersion (b) and H/V ratio curves (c). Fig. a: Tested models (grey lines), the minimum cost model (white line), and models lying inside the minimum cost + 10% range (black lines). Fig. b-c: observed (grey circles) and for the minimum cost model (white circles).

In Figure 26a tested models are depicted in different colours according to their relevant cost value: in white the more reliable model (minimum cost); in black models lying inside the 10% range of the minimum cost; while others tested models are shown with the grey colour. Best model V_S profile appears to be well constrained between 10 to 40 m. The good agreement between experimental and theoretical Rayleigh wave dispersion curves (Figure 26b) assures on the credibility of the V_S profile down to about 100 m.

The deep part of the profile (over 300m depth) and the impedance contrast between the clayey formation and the bedrock are constrained using NHV. However, in this case, the only approximate fitness of the NHV curve indicates lower reliability of the results (Figure 26c), as also shown by the larger scattering of the profiles below 100 m (Figure 26a).

In particular, two families of profiles are predicted by the inversion procedure to describe the deepest part of the model: the first propose that the deep clay layer has a V_S of 500 m/s and that the bedrock is located at nearly 440 m with a V_S of 900 m/s; the second estimate a V_S of 600 m/s for the clayey formation in proximity of the bedrock which is characterized by 1500 m/s in terms of V_S and it is located at 560 m depth. We are inclined to consider the second family of profiles as the more reliable, because it was already predicted by other inversion analyses − not reported here − while changing the weight *p* (equal to 0.02 and 0.05).

In the V_S profile of Figure 26a two velocity inversions are present at 10 and 50 m of depth, and probably higher modes became predominant.

Love waves are expected to be more sensitive with respect to velocity inversions. For this reason Love wave dispersion curve analysis is expected to improve the reliability of the estimation of shear wave velocities assigned to upper layers and it will be carried out in the following.

Love wave dispersion curve analysis

The Love waves experimental dispersion curve was obtained after applying the f-k spectral method to decomposed transversal horizontal (that is supposed to be dominated by Love waves) components of microtremor records. Transversal horizontal component is the projection on the estimated predominant azimuths of the microtremor sources. A clearer Love-wave dispersion curve with lower standard deviation was obtained applying the *f-k* spectral method (beam forming). The average observed Love-wave dispersion curve is displayed in Figure 27 as 20 red points in the frequency range of 1.3 – 3.2 Hz. It is computed using a software developed by the Natural Research Institute for Earth Science and Disaster Prevention of Japan, on the basis of 12 sets composed by 11 (BE2 – BE12), 80 s synchronized traces of microtremor. In the same figure. 10 % of the average Love-wave phase velocity at each frequency is also shown with “black hyphen”.

The same 12 sets of microtremor synchronized traces were used to estimate Rayleigh-wave dispersion characteristics by the *f-k* spectral method (Figure 27). A narrow frequency band with high standard deviation was obtained in the observed Rayleigh-wave dispersion curve.

For the inverse analysis, a geotechnical model consisting in 4 horizontal layers overlying a half-space was used (Table 3). A random search (Monte Carlo inversion) on three parameters (thickness, S-wave velocity and Poisson’s ratio) for each layer was used. The other properties of each layer, such as the P-wave velocity and the density, were calculated after defining the values of the 3 random parameters (Tokeshi et al., 2008).

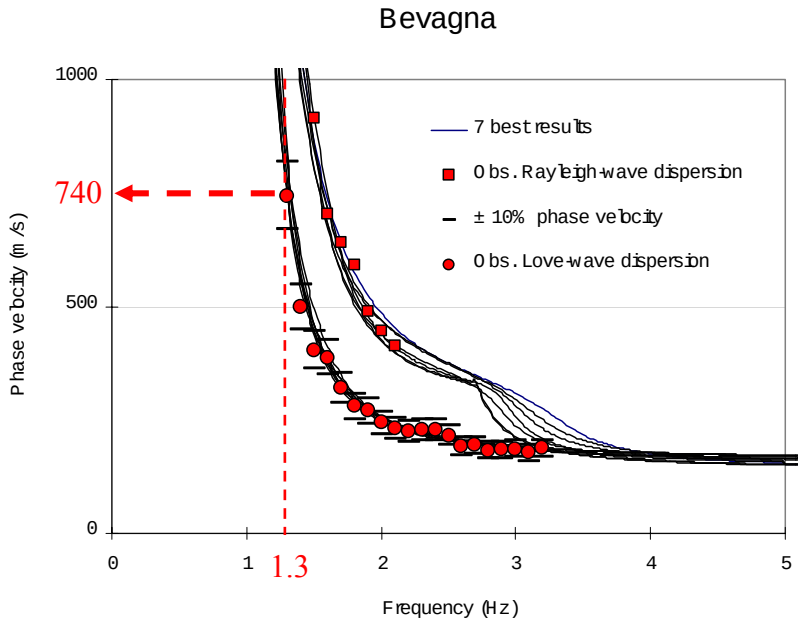

Figure 27 – Comparison of observed and theoretical Love-wave / Rayleigh-wave fundamental modes.

One million trials were performed during random search, and in order to improve the efficiency of the algorithm, the value of the SH-wave resonant frequency at each trial was calculated. Only the random models whose resonance frequencies were lower than the threshold frequency of 1.3 Hz proceeded to the next step. Then, the theoretical Love-wave fundamental mode for each geotechnical model was compared with the observed one, by checking the number of points where the phase velocity of Love-wave fundamental mode is within the relative error of 10% of the observed phase velocity. After the random search, the possible geotechnical models were lined up according to the number of points satisfying the previous condition, and to the least-square-misfit criterion.

	Poisson's ratio, ν		S-wave velocity, V_S [m/s]		Thickness, h [m]	
Layer	MIN	MAX	MIN	MAX	MIN	MAX
1	0.25	0.49	100	400	1	30
2				700		100
3				1000		100
4				1500		100
Half-space		V_S = 2500		V_P = 3800		Infinite

Table 3 – Ranges used in parameters for random inverse analysis.

Figure 27 displays the comparison between the observed (red circles) and the theoretical (black lines) Love fundamental dispersion curves of the 7 best solutions (Figure 28b) that satisfied the condition for the 20 points (all frequencies). In addition, the comparison between the observed and the theoretical Rayleigh fundamental modes associated to these 7 geotechnical models is represented in Figure 27. There is good agreement between observed and theoretical Love/Rayleigh-waves fundamental modes.

Comparison of Rayleigh and Love waves analyses with other tests available in the study area

The results obtained from the separated Rayleigh (Figure 28a) and Love (Figure 28b) waves inversions analyses showed that the two procedure provide consistent shear wave velocity profiles for the shallow part of the model where they can be directly compared. These profiles are in good agreement with the results of the nearby Cross-Hole (CH) test, which were carried out at BVG site in the framework of the DPC-INGV S6 Project (Luzi and Sabetta, 2006), offering the opportunity to compare the subsoil velocity profiles derived by seismic noise array data with independent geophysical information.

Rayleigh wave analysis, which was performed taking into account higher modes, shows a satisfactory agreement with the CH test results. In fact, it is able to reproduce well the velocity trend (including the inversion at 10 m depth), although it underestimates the V_S measured with respect to the CH test results at depth ranging from 20 to 30 m On the contrary Love wave analyses does not evidenced velocity inversions probably because only the fundamental mode of the soil deposit is used. In general, the assumed geotechnical models follow very close the cross-hole measurements. Estimated soil profiles by Love wave analysis are consistent with those obtained by Rayleigh wave inversion down to 60 m when phase velocities for all layers are lower than 740 m/s (at 1.3 Hz in Figure 27 ???).

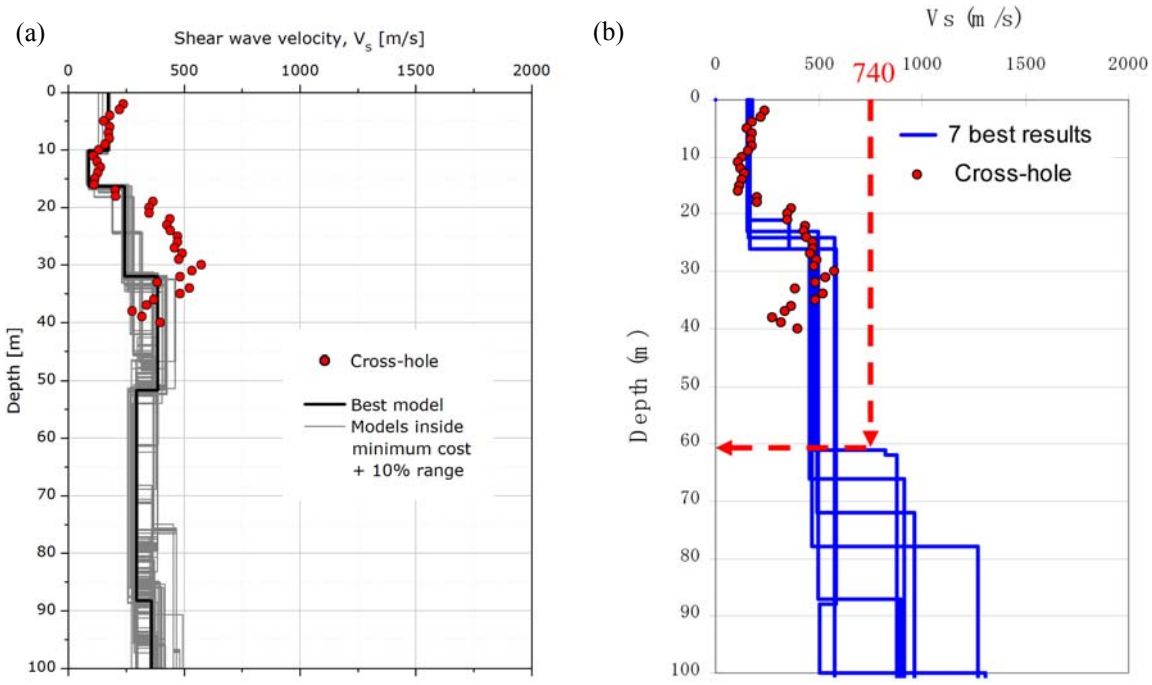

Figure 28 – Comparison between cross-hole and Vs soil profiles based on observed Rayleigh (a) and Love (b) dispersion curves. In the Rayleigh analysis also higher modes are taken into account, while the Love inversion is performed on fundamental mode.

Furthermore a seismic refraction survey (Figure 29) was executed within the DPC-INGV S6 Project (Luzi and Sabetta, 2006). It also highlights the seismic impedance contrast in the clay formation at about 20 m of depth which was estimated by both the inversion procedure here applied.

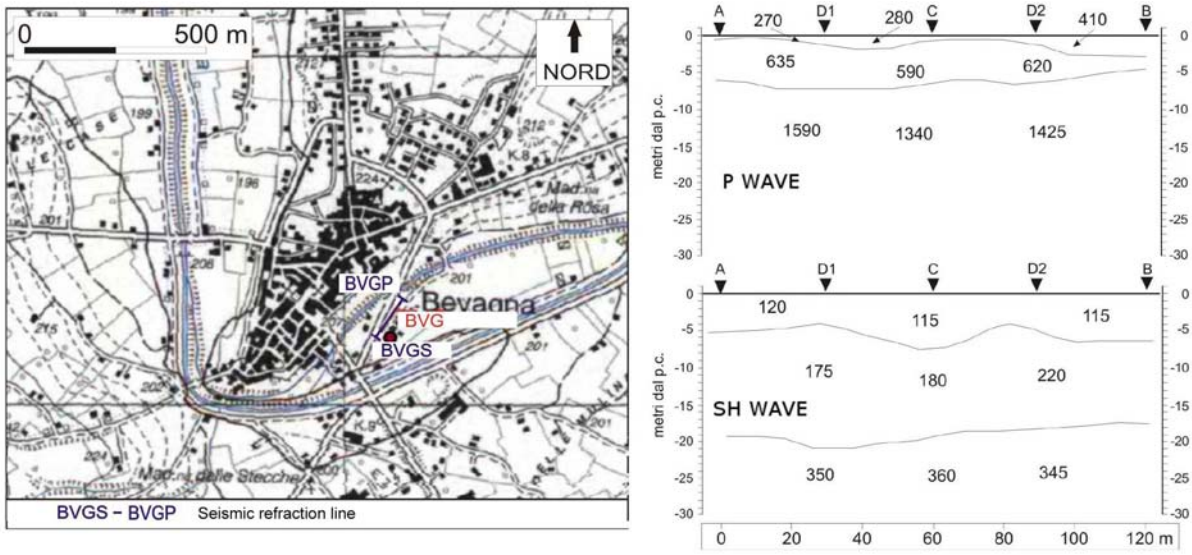

Figure 29 – Seismic refraction line results at the BVG station.

This case history shows the capability of surface wave analysis from passive source to adequately retrieve the S-wave subsoil structure and it suggests that more efforts should be devoted in exploiting the potential of coupled analysis of Rayleigh and Love waves from microtremor array measurements for site characterization.

5.2 Shallow bedrock sites of RAN in Liguria

Active surface wave tests (MASW) at 4 sites in Liguria have been performed in October 2008 within the project S4 for the characterization of RAN sites. Data have been collected using 48 4.5 Hz vertical geophones and a sledge-hammer as a source. The spacing of geophones has been dictated by available testing space at the testing locations, which was typically very limited because the stations are placed in urbanised areas.

All the RAN stations in Liguria were classified as rock outcrop and a very limited zone of rock alteration and vegetation soil was expected above the bedrock. In this situation the synergies between surface wave active methods and P-wave refraction surveys are relevant. Indeed both surveys can be performed with the same testing configuration or even the same experimental data can be used for both interpretations (Foti et al., 2003). In particular P-wave seismic refraction method can in this situation provide relevant information with respect to the position of the interface between the soil cover and the bedrock. This information can be used as an a-priori information for the inversion of surface wave data aimed at retried the shear wave velocity profile.

In surface wave analysis it is very common to perform the inversions using only the fundamental mode of propagation. This approach is based on the assumption that the prevailing mode of propagation is the fundamental one; if this is partially true for normal dispersive sites, in several real cases the experimental dispersion curve is on the contrary the result of the superposition of several modes. This may happen in particular when velocity inversions or strong velocity contrasts are present in the shear wave velocity profile. In these stratigraphic conditions the inversion of the only fundamental mode will produce significant errors; moreover all the information contained in higher propagating modes is not used in the inversion process. Therefore, the fundamental mode inversion does not use all the available information, and this affects the result accuracy.

The use of higher modes in the inversion can be helpful both in the low frequency range, in order to increase the investigation depth and to avoid the overestimation of the bedrock

velocity, and in the high frequency range in order to provide a more consistent interpretation of shallow interfaces and increase model parameter resolution. The algorithm used to perform dispersion curve inversion in the present work is a stochastic algorithm which makes use of a multimodal error function based on the minimization of a misfit distance related to the Haskell-Thomson determinant (Maraschini et al., 2008). The inversion method adopted has the advantage of being able to include any dispersive event present in the data without the need of specifying to which mode the data points belong to. Ranges for the stochastic inversion have been chosen, for the different sites, based on the experimental dispersion curves; in particular the range of the S-wave half space velocity is close to the maximum surface wave velocity retrieved on experimental data.

The results of the inversion are reported as the ensemble of the twenty shear wave velocity profiles which present the minimum misfits with respect to the experimental dispersion curve. In the figures reported for each case history a representation based on the misfit is adopted for velocity profiles, so that the darkest color corresponds to the profile whose dispersion curve has the lowest misfit and better approximation to the reference one; instead for dispersion curves the colored surface under imposed to the experimental one (white data points) is a misfit surface, whose zeros are synthetic dispersion curve of the best fitting model. Observing the different figures, we can note that observed dispersion curve points are placed in the minimum of the misfit function.

Example 1 – Sestri Levante Site.

The visual inspection of the site reveals the presence of a compacted superficial layer (gravels and pebbles) which is a track for the passage of trucks. The dispersion curve acquired for the site (Figure 30-b) indeed shows a peculiar increase in velocity with frequency. This transition clearly reveals that the propagation progressively shifts to higher modes for increasing frequency and thus that a probable velocity inversion would be present in shallow layers. The results of the inversion are reported in Figure 30-a well underlining the potentiality of a proper consideration of this higher modes behaviour. Indeed all profiles selected by the stochastic process (Figure 30-a), which are by the way extremely coherent, reveals the presence of a more compacted stiff layer in the shallow surface and the presence of a velocity inversion before the bedrock is detected. Accounting for higher modes in the inversion process for this site is also relevant to extend the depth of investigation (frequencies below 20 Hz) and to estimate correctly depth and shear wave velocity of the bedrock.

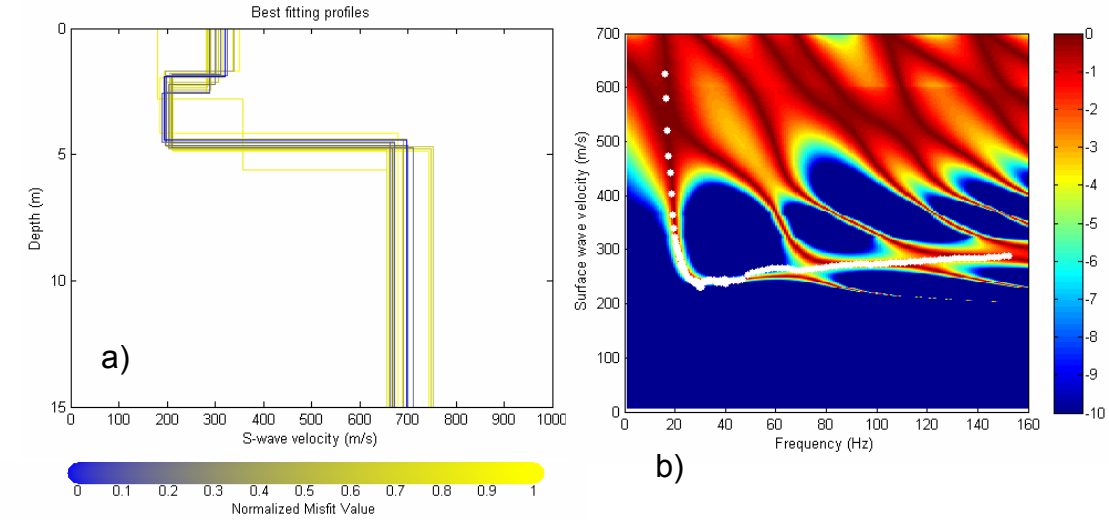

Figure 30 – Sestri Levante Site: a) Profiles selected by the MonteCarlo inversion; b) Dispersion curve.

Example 2 – Varese Ligure site

In this and in the following site a shallow seismic refraction profile has been addittionally performed in order to provide a further element in the interpretation of the seismic stratigraphy. The advantages of combining surface wave and P-wave seismic refraction methods are also given by the possibility of using the same testing setup. Particularly the positions of seismic interfaces are compared between the two methods providing a more reliable estimate of bedrock position (even if the inversion process of surface wave data has been performed independently). For this case history the use of low frequency data points in the dispersion curve that likely belong to higher propagating modes is essential to increase investigation depth (Figure 31-b). Indeed for the experimental data below 40 Hz the dispersion curve reveals a progressive transition towards an higher mode of propagation; using this data points, that would be discharged in an interpretation based only on the fundamental mode of propagation, it is possible to correctly delineate the bedrock depth and velocity. Results of the inversion (Figure 31-a) shows a good match with the interfaces revealed by the interpretation of the refraction shots; only in the location of the second interface there is an increased uncertainty revealed by the different profiles selected by the stochastic process. Again even if this appears to be a normal dispersive site the presence of strong and relatively shallow contrast in the shear wave velocity profile reveals the need for accounting for higher modes.

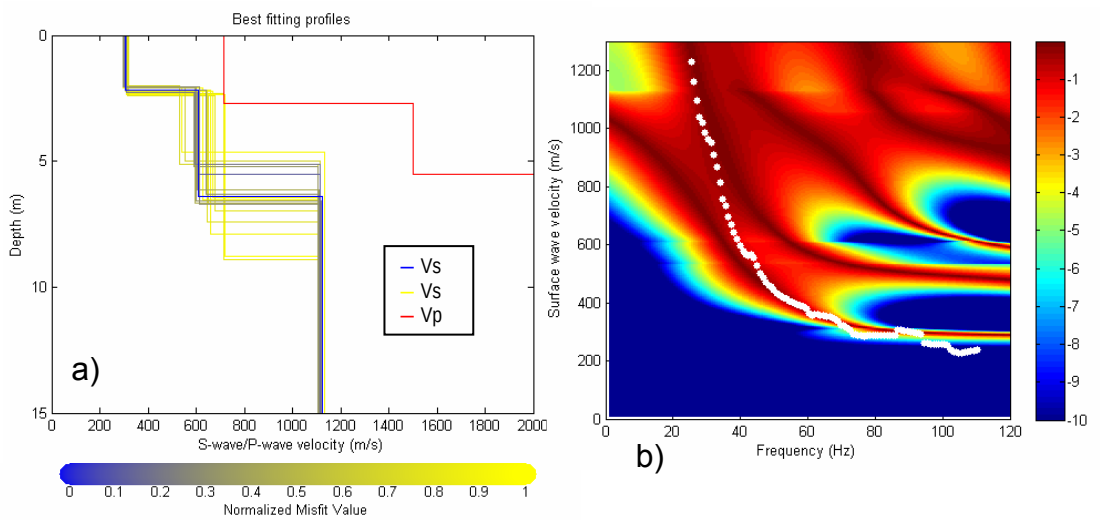

Figure 31 – Varese Ligure Site: a) Profiles selected by the MonteCarlo inversion and seismic refraction interpretation; b) Dispersion curve.

Example 3 – Genova site

The experimental dispersion curve for this site reveals a significantly high frequency content in the experimental data (Figure 32-b); two different branches were clearly visible in the f-k spectra of the traces.

As mentioned the inversion algorithm adopted does not need to specify to which mode the data points have to belong so that both modes could be used without any particular specification in the inversion. Indeed in this site the emerging bedrock was clearly visible in the vicinity of the accelerometer station and only a very shallow coverage could be noticeable in the zone where tests have been executed. The detailed definition of the shallow stratigraphy is therefore based on the acquisition of high frequency components of the dispersion curve. Again a good correspondence with refraction data is obtained in the location of the first interface (Figure 32-a).

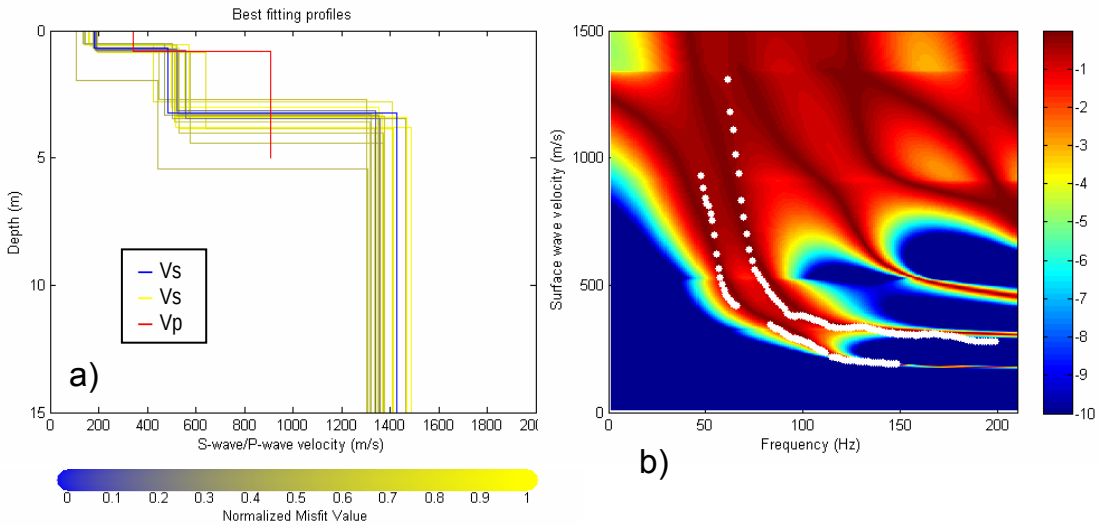

Figure 32 – Genova Site: a) Profiles selected by the MonteCarlo inversion and seismic refraction interpretation; b) Dispersion curve.

5.3 SASW tests by USGS in Umbria-Marche sites

17 strong motion instrument sites for which records from the umbria-Marche seismic sequence of 1997-1998 are available have been tested using the two-station SASW method by USGS within an independent research project (Kayen et al., 2008). The comparison of the SASW results at some sites of the RAN network for which borehole seismic test results were available (Gubbio Piana, Norcia, Colfiorito, Sellano) showed marked difference especially for some soft soil deposits for which Kayen et al. (2008) reported quite high values of shear wave velocity.

The inspection of USGS report (Kayen et al., 2008) showed for several sites some inconsistencies in particular with respect to the two following aspects:

1) the experimental dispersion curves from different testing configuration at the same site were not consistent in several cases;

2) the fitting between the experimental dispersion curve and the numerical dispersion curve for the last iteration of the inversion process were not satisfactory at several sites.

Based on the comparison with borehole seismic tests, it has been recognised that at low velocity sites an error was introduced in phase unwrapping (Kayen et al., 2009). Indeed SASW tests at Umbria-Marche sites were performed with a controlled source (an electro-mechanical shaker) used in a stepped-sine mode and the tested frequency range was such that the first phase jump in the wrapped cross-power spectrum phase was missed (see Figure 5-top). Moreover the use of a common source acquisition scheme (see Figure 6b) made the experimental results prone to instrumental errors.

Experimental data have been successively reprocessed forcing one full phase jump (360°) at low frequency in the phase unwrapping at slow sites, leading to more consistent results (Kayen et al., 2009). However, due to the strong subjectivity in tuning the results after having a-posteriori corrected the phase difference, the soil profiles obtained by SASW tests will be considered in this project only (and with care) if other in-situ measurements are not available. An example of the original dispersion curves and the modified ones for the same experimental dataset is reported in Figure 33. The difference on the estimated shear wave velocity profile

which is associated to the problems with phase unwrapping can be quite substantial (see for example the comparison in Figure 34). These surveys show the errors that can be introduced by phase unwrapping in the two-station SASW approach, which make this approach not recommended for active surface wave tests. In any case it has to be recalled that two-station phase difference measurements are very sensitive to instrumental errors, so that a careful tuning of the receivers and the adoption of the common-source acquisition scheme (see Figure 6a) are suggested.

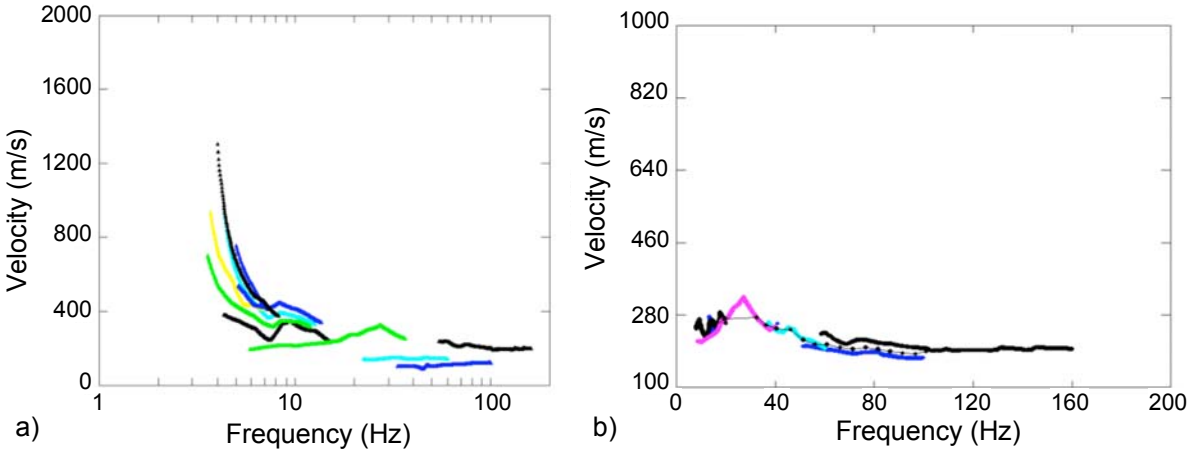

Figure 33 – Experimental dispersion curves from SASW tests at Colfiorito Site: a) original data processing (USGS, 2008); b) data reprocessing with the introduction of an additional phase jump in the cross-power spectrum phase (USGS, 2009).

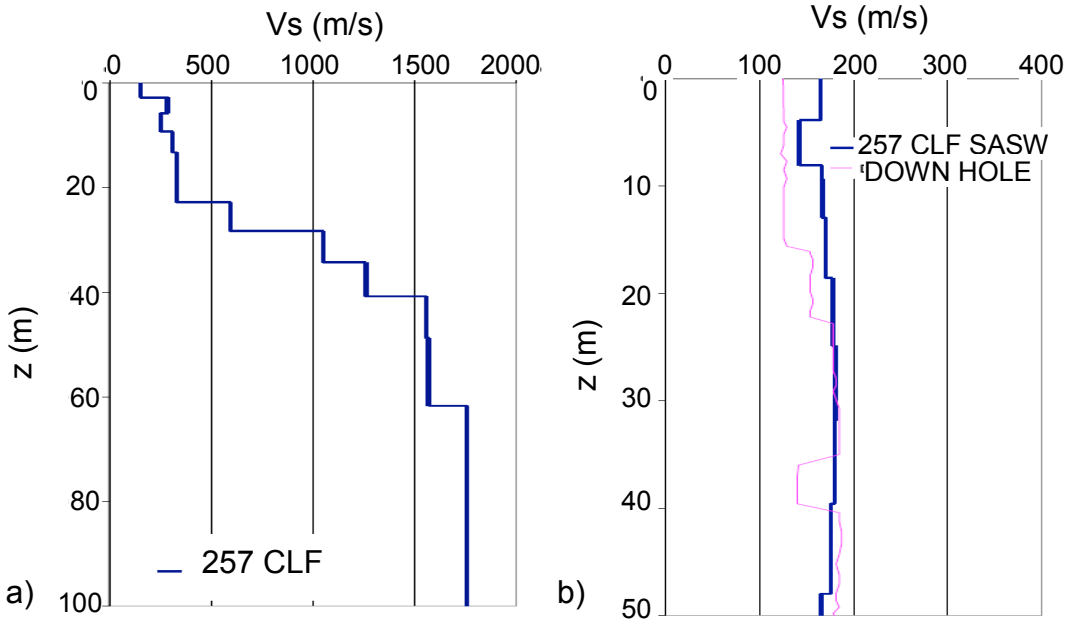

Figure 34 – Shear wave velocity profiles from SASW tests at Colfiorito Site: a) original data processing (USGS, 2008); b) data reprocessing with the introduction of an additional phase jump in the cross-power spectrum phase (USGS, 2009).

6. Recommendations

6.1 Limitations and advantages of surface wave tests

Advantages of surface methods are mainly related to their non-invasive nature. They are more economical and can be performed more rapidly than borehole methods. Furthermore, in sites like solid waste disposals and landfills, due to environmental concerns, surface methods can be the only choice for geotechnical investigations. Another peculiar aspect of surface methods is related to the volume of soil involved in the test, which is much larger than in borehole methods. As a result, surface methods are particularly useful if the average properties of a soil deposit are to be assessed as in the case of ground response analyses.

A major limitation of surface wave method is related to the model that is used for the interpretation. Typically a stack of linear elastic layers is used as a model, hence surface wave tests cannot identify lateral variation and the final result is biased if the soil deposit does not resemble reasonably a layered medium. Several approaches proposed for the construction of 2D models from surface wave data are still based on a set of 1D inversions and as a such they should be used with particular care and with a clear understanding of the actual procedure (Socco et al., 2009). However, the seismic interferometry approach of Picozzi et al. (2009) seems to be promising with respect of the capability of estimating 2 or 3D subsoil structure with surface wave analysis.

Because inverse problems are mathematically ill-posed, the non uniqueness of the solution plays a role. Indeed several profiles which give numerical dispersion curves having a similar distance from the experimental dispersion curve can be identified. This problem is well known as equivalence in geophysical tests based on inverse problems. The implications are a certain degree of uncertainty in the final shear wave velocity profile. For example surface wave test are not the first choice is the objective is the exact location of an interface between different layers.

The resolution in the shear wave velocity profile that can be obtained with surface wave is decreasing for increasing depth. Thin layers can be resolved if they are close to the ground surface, but they are not “seen” by the method if they are at depth.

Still surface wave methods provide an excellent tool for soil characterization if the overall behaviour of the medium has to be identified. Their main advantage comes from the non-invasive nature of the test: all the measurements are performed from the ground surface with no need for boreholes. For this reason they are cost and time effective (no need for preparation) and can be performed where it is not advisable to invade the medium (e.g. waste disposals).

Compared to seismic refraction using horizontally polarized shear waves, which is another test to get the shear wave velocity non-invasively, surface wave tests do not suffer limitations related to the actual site stratigraphy, being able to characterize the medium independently from the actual sequence of stiffer (faster) and softer (slower) layers. Indeed refraction methods suffer for the presence of hidden layers having certain ratios of thickness and/or velocity, which makes them not detectable using such techniques.

Performances of surface wave tests are good even in noisy environments (e.g. urban areas or industrial sites). Other seismic tests based on the evaluation of first arrivals and travel time are much more difficult to interpret in presence of background noise. The processing of surface wave data is entirely done in the frequency domain. The presence of excessive noise for specific frequencies does not compromise the possibility of interpreting the data. Background

noise can even be used as a source of information using microtremors surveys. In particular, this kind of analysis has the advantage to allow investigations to very large depths (hundred meters to kilometres) that would be prohibitive with active source methods due to the lack of energy with standard sources in the low frequency range. Therefore, surface wave methods based on seismic noise analysis are particularly attractive for studying subsoil structure in urban areas and deep sedimentary basins.

Large volumes of soils are tested and the test results reflect the overall dynamic behaviour of the soil deposit. The degree of accuracy obtained with surface wave test is typically in line with the assumptions and the simplifications adopted in the design stage. Moreover the 1D model used for the interpretation is also common for many engineering approaches for design and verification (as for example the code Shake for the evaluation of the seismic response of the site, see Foti et al., 2009).

The selection of appropriate technique (active, passive, active+passive) for the site is related to the objective of the characterization: active methods are best suited for high resolution shallow characterization, whereas passive methods provide a greater penetration depth, but limited resolution close to the ground surface. In situations where both these scopes (deep characterization and high resolution at shallow depth) have to be persecuted, the combination of both active and passive data give the optimal result (Richwalski et al., 2007; Foti et al., 2009).

The choice of specific approaches for acquisition, processing and inversion within each testing technique is strongly linked to available instruments and specific experience of the operator. Although in principle all methods, if carefully applied, should yield to sufficiently reliable results, the following general suggestions can be provided:

- ⇒ As active tests are concerned, the 2-station method is not preferable because its interpretation in noisy environment and for complex sites can be not straightforward. In particular the process of phase unwrapping can lead to substantial errors and requires a good experience of operator. Moreover it has to be considered that the phase difference measurement can be affected by instrumental error and the standard testing procedure (common receiver midpoint) is quite consuming on site;
- ⇒ As passive tests are concerned, the use of ReMi method has to be avoided because it relies on the strong assumption on the homogeneous distribution of sources and the picking of intermediate points in the f-p (or f-k) spectrum is operator dependent. Would ReMi methods be used anyway, it is suggested to combine data acquisition with active MASW data, since the testing setup is the same and only some shots with an active source (for shallow depth of investigation just a sledge hammer) are required;
- ⇒ For the inversion of surface wave data, the influence of higher modes in the propagation has to be carefully taken into account and the use of global search methods is suggested, especially for sites very the complexity of geology or the observation of the experimental dispersion curve make the possibility of being trapped in local minima in the inversion process are relatively high;

6.2 Some notes on the characterization of sites on outcropping rock

The seismic characterization of stiff-soil and rock-mass sites (behaving as seismic bedrock) represents a critical aspect for effective and proper location of seismic and accelerometric stations and for the analysis of seismic response by using the reference station approach. In general, it is assumed that flat rock and stiff soil sites represent an ideal location where

possible near surface amplification effects can be excluded. However, this assumption is not consistent with widespread evidence of rock and soil alteration phenomena induced by faulting, jointing and weathering. These phenomena could be responsible for significant modifications of dynamic properties of the subsoil both in the vertical direction and laterally. In particular, they can alter the seismic response at the site due to the presence of Vs velocity contrasts.

In general, presence of vertical variations can be easily revealed by point-wise NHV measurements and the relevant Vs profile can be constrained by jointly inverting NHV and surface waves dispersion curves obtained by array measurements nearby the station. However, as it concerns the latter, some critical aspects should be accounted for. In the presence of relatively high phase velocities (such the ones expected at stiff and rock-mass sites), large wave lengths with respect the overall dimension of the array are expected in the frequency range commonly considered for this kind of analysis (5-20 Hz to say). Thus, relatively small phase differences are expected at most of the array receivers: being V_r the average velocity, the smallest inter-geophonic distance Δx_{min} able to provide a velocity value at the sampling frequency ν is V_r/ν. This implies that aliasing occurs for wavelengths smaller than $2\,\Delta x_{min} = 2\,V_r/\nu$. Furthermore, in the case that most of the inter-geophonic distances of the array are smaller than $2\,\Delta x_{min}$, all the wavelengths above this value result undersampled from the statistical point of view. The longest resolved wavelength is of the order of the overall dimension D of the array and this last dimension also limits the resolving power of the array in the wavenumber domain: this last limitation is as more significant as larger are the involved wavelengths and phase velocities. As an effect of these limitations (especially the finiteness of the sampling rate), the dispersion curve deduced from array measurements assumes a characteristic saw-tooth shape that masks the underlying smooth pattern and makes difficult a physically plausible interpretation. To improve the performances of the array, sampling rates should be increased with respect to common standards (from 128 to 512 Hz to say) along with the overall dimensions of the array. However, as concerns this last possibility, severe limitations are posed by available instrumentation and free space.

As it concerns the detection of lateral variations in the subsoil dynamical properties, exploratory NHV measurements driven by geologic indications can allow a preliminary mapping of possible different dynamical behaviour of the geologic bodies present around the station. Interferometric interpretation of array measurements could also help in the identification and characterization of existing lateral heterogeneities.

6.3 Selection of sites to be investigated

The selection of site of the RAN to be classified by using surface wave based methods was driven by several criteria. First, as general criteria, the attention was pointed to stations that recorded interesting events in the past and to the recently installed digital stations. Moreover, it was paid attention to have a good coverage for the whole Italian territory, excluding regions with a higher availability of results from previous surveys.

Considering specific criteria relevant to the adopted technique for estimating the S-wave velocity structure below the site, it was decided, on the basis of a preliminary analysis of the ITACA station monigraphies and with the help of Google Earth imagine analysis to exclude site with complicated topography and with no sufficient space for carrying out the surface wave measurements.

The large set of sites that remained was then inspected through field investigations that allowed to define a nearly-final list of selected sites. The preliminary field investigations were meant at verifying the suitability of the sites for surface wave method investigation. Drawing the ultimate list of the investigated sites will be possible only after the field measurement

campaign since due to logistic problems, some changes are still possible. A map of the site selected for the preliminary field inspection is shown in Figure 35.

Figure 35 – Map showing the sites that have been selected for a preliminary in-situ investigation. This field inspection is meant at verifying the suitability of the sites for the surface wave method investigation.

Finally, considering the ´geological characteristics of the selected sites (thin, i.e. meters/tens of meters of soft sediments, or thick, i.e. hundreds of meters of soft sediments) it was decided to assign them amongst the different UR involved in the work package by considering their expertise. In particular, it was decided that thin sedimentary covers sites were assigned mainly to UR with large experience in active methods and with appropriate instruments (multi-channel acquisition systems with high frequency geophones) while the deep basins were assigned to the URs with large experience in passive source methods and equipped with short period seismometers.

Considering the target of the survey, different strategies will be used. For example at sites with very shallow bedrock (as for example in Liguria and in the south-east of Sicily, where only thin rock alteration zone are present close to the ground surface waves) only active surface wave tests with multistation testing setup (MASW) are going to be used. At site with very deep bedrock, as for example in the Po Plain, only passive methods with 2D arrays are going to be used. In intermediate situations, a combination of active and passive methods will

be used to guarantee adequate depth of exploration and good resolution at shallow depth. Moreover, selected rock sites will be thoroughly investigated to assess the effects of faulting, jointing and weathering with a combination of surface wave surveys and classical geomechanical approaches.

7. Relevance for DPC and/or for the scientific community

The present deliverable is intentended to provide the basis for the selection of appropriate techniques for the characterization of sites of the italian accelerometric network and for projects related to seismic site response studies (e.g. for microzonation).

8. References

Aki, K., 1957. Space and time spectra of stationary stochastic waves, with special reference to microtremors, *Bull. Earthq. Res. Inst.*, 35, 415-456.

Aki, K.,1965, A note on the use of microseisms in determining the shallow structure of the Earth's crust*: Geophysics*, 30, 665-666

Aki K., Richards P.G. 1980. Quantitative seismology: theory and methods - 2 vol. Freeman. S. Francisco

Albarello D. and Lunedei E., 2009. Alternative interpretations of Horizontal to Vertical Spectral Ratios of ambient vibrations: new insights from theoretical modeling. Bull.Earthq.Engng., DOI: 10.1007/s10518-009-9110-0

Arai, H., and K. Tokimatsu 2000. Effects of Rayleigh and Love waves on microtremor H/V spectra, paper presented at *12th World Conference on Earthquake Engineering*, N. Z. Soc. for Earthquake Eng., Auckland, N. Z.

Arai, H., and K. Tokimatsu 2004. S-wave velocity profiling by inversion of microtremor H/V spectrum, *Bull. Seism. Soc. Am*. 94, 53–63.

Arai, H. and K. Tokimatsu 2005. S-wave velocity profiling by joint inversion of microtremor dispersion curve and horizontal-to-vertical (H/V) spectrum. *Bull. Seism. Soc. Am.* 95, 1766-1778.

Bakulin, A. & Calvert, R., 2004. Virtual source: new method for imaging and 4D below complex overburden, in *Proceedings of 74th Annual International Meeting*(expanded abstracts), Society of Exploration Geophysicists, 2477–2480.

Bakulin, A. & Calvert, R., 2006. The virtual source method: theory and case study, *Geophysics,* 71, S1139–S1150.

Bard, P. Y. 1998 Microtremor measurement: a tool for site e_ect estimation? Second International Symposium on the Effects of the Surface Geology on Seismic Motion ESG98, Japan.

Ben-Menahem A., Singh S.J., 2000. Seismic waves and sources, Dover Publications Inc., New York, 1102 pp.

Birtill, J.W., and Whiteway, F.E., 1965. The application of phased arrays to the analysis of seismic body waves, *Philos. Trans. R. Soc. London*, Ser. A, 258, 421-493.

Buchen, P.W. and Ben-Hador, R., 1996. Free-mode surface-wave computations, *Geophys. J. Int.,* **124,** 869–887.

Campillo,M. and Paul, A., 2003. Long-range correlations in the seismic coda, *Science,* 299, 547–549.

Capon, J., 1969. High-resolution frequency-wavenumber spectrum analysis, *Proc. IEEE*, 57, 8, 1408-1418.

Chavez-Garcıa, F.J. & Luzon, F., 2005. On the correlation of seismic microtremors,*J. geophys. Res.,* 110, B11313, doi:10.1029/2005JB003671.

Chavez-Garcıa, F.J. & Rodrıguez, M., 2007. The correlation of microtremors: empirical limits and relations between results in frequency and time domains, *Geophys. J. Int.,* 171, 657–664.

Cho, K.H., Herrmann, R.B. & Ammon, C.J. & Lee, K., 2007. Imaging the upper crust of the Korean Peninsula by surface-wave tomography, *Bull. seism. Soc. Am.,* 97, 198–207, doi:10.1785/0120060096.

Curtis, A., Gerstoft, P., Sato, H., Snieder, R. &Wapenaar, K., 2006. Seismic interferometry—turning noise into signal, *Leading Edge,* 25, 1082–1092.

D'Amico V., Picozzi M., Albarello D., Naso G. and Tropenscovino S., 2004. Quick estimate of soft sediments thickness from ambient noise horizontal to vertical spectral ratios: a case study in southern Italy". J. Earthq. Engineering, 8, 6, 895-908

D'Amico V., Picozzi M., Baliva F. and Albarello D., 2008. Ambient Noise Measurements for Preliminary Site-Effects Characterization in the Urban Area of Florence. *Bull.Seism.Soc.Am.,* 98, 3, 1373-1388, doi: 10.1785/0120070231

Delgado, J., C. Lopez Casado, A. C. Estevez, J. Giner, A. Cuenca and S. Molina 2000a. Mapping soft soils in the Segura river valley (SE Spain): a case study of microtremors as an exploration tool, *J. Appl. Geophys.* 45, 19–32.

Delgado, J., C. Lopez Casado, J. Giner, A. Estevez, A. Cuenca, and S. Molina. 2000b. Microtremors as a geophysical exploration tool: applications and limitations, *Pure Appl. Geophys.* 157, 1445–1462. 1841.

Dong, S., He, R. & Schuster, G., 2006. Interferometric prediction and leastsquares subtraction of surface waves, in *Proceedings of 76th Annual International Meeting* (expanded abstracts), Society of Exploration Geophysicists, 2783–2786.

Douglas, A., 2002. Seismometer arrays – Their use in earthquake and test ban seismology, in *Handbook of Earthquake and Engineering Seismology*, edited by P. Jennings, H. Kanamori, and W. Lee, 357-367, Academic, San Diego, Calif.

Dziewonski A.M., Hales A.L. 1972. Numerical Analysis of Dispersed Seismic Waves. In Methods in Computational Physics vol.11 Seismology: Surface waves and Earth Oscillations. Bolt, B.A. Ademic Press. New York: 39-85

Fäh, D., Kind, F., and Giardini, D., 2001, A theoretical investigation of average H/V ratios: Geophys. J. Int., 145, 535-549.

Fäh, D., Kind, F., and Giardini, D., 2003, Inversion of local S-wave velocity structures from average H/V ratios, and their use for the estimation of site-effects: J. Seismology, 7, 449-467.

Field, E. H. and Jacob, K. 1993 The theoretical response of sedimentary layers to ambient seismic noise", Geophys. Res. Lett. 20 24, 2925 2928.

Foti S., 2000. Multistation Methods for Geotechnical Characterization using Surface Waves. PhD dissertation, Politecnico di Torino, Italy

Foti S., 2003. Small Strain Stiffness and Damping Ratio of Pisa Clay from Surface Wave Tests. Geotechnique, 53(5): 455-461

Foti S., 2004. Using Transfer Function for Estimating Dissipative Properties of Soils from Surface Wave Data. Near Surface Geophysics, EAGE, vol. 2 (4), 231-240

Foti S. 2005. Surface Wave Testing for Geotechnical Characterization. in *Surface Waves in Geomechanics: Direct and Inverse Modelling for Soils and Rocks*, CISM Series, Number 481, Lai C.G. and Wilmanski K. eds, Springer, Wien, 47-71

Foti S., Lancellotta R., Sambuelli L., Socco L.V., 2000 "Notes on fk analysis of surface waves", Annali di Geofisica, vol. 43, n.6, 1199-1210

Foti S., Comina C., Boiero D., Socco L.V., 2009 "Non uniqueness in surface wave inversion and consequences on seismic site response analyses", Soil Dynamics and Earthquake Engineering, Vol. 29 (6), 982-993

Foti S., Sambuelli L., Socco L.V., Strobbia C., 2003 Experiments of joint acquisition of seismic refraction and surface wave data, Near Surface Geophysics, EAGE, 119-129

Frosch, R.A., and Green, P.E., 1966. The concept of the large aperture seismic array, *Proc. R. Soc. London*, Ser. A, 290, 368-384.

Gabriels P., Snieder R., Nolet G., 1987. In situ measurements of shear-wave velocity in sediments with higher-mode Rayleigh waves. Geophys. Prospect. 35: 187-196

Ganji V., Gukunski N., Nazarian S., 1998 "Automated inversion procedure for spectral analysis of surface waves", J. Geotech. and Geoenv. Eng., vol. 124, ASCE, pp. 757-770

Gerstoft P., Sabra K.G., Roux P., Kuperman W.A. & Fehler M.C., 2006. Green's functions extraction and surface-wave tomography from microseisms in southern California, *Geophysics,* 71, 23–32.

Goldberg D.E., 1989, Genetic algorithms in Search, Optimization and Machine Learning: Addison-Wesley.

Halliday D.F. & Curtis A., 2008a. Seismic interferometry, surface waves, and source distribution, *Geophys. J. Int.,* doi:10.1111/j.1365- 246X.2008.03918.x.

Halliday D.F. & Curtis A., 2008b. Seismic interferometry of scattered surface waves in attenuative media, submitted.

Halliday D.F., Curtis A., Robertsson J.O.A. & van Manen D.-J., 2007. Interferometric surface-wave isolation and removal, *Geophysics,* 72, A67–A73.

Halliday D.F., Curtis A. & Kragh E., 2008. Seismic surface waves in a suburban environment—active and passive interferometric methods, *Leading Edge,* 27, 210–218.

Harkrider D.G., 1964. Surface waves in multi-layered elastic media. I Rayleigh and Love waves from buried sources in a multilayered elastic half space. *Bull. Seism. Soc. Am.* 54, 627–679.

Herrmann, R.B., 1987. *Computer Programs in Seismology,* Vol. IV, St. Louis University, MO, USA.

Herrmann R.B., C.J. Ammon, J. Julia, and T. Mokhtar (1999). Joint inversion of receiver functions and surface-wave dispersion for crustal structure. Proc. 21st Seismic Research Symposium Technologies for monitoring the comprehensive Nuclear test Ban treaty, September 21-24, 1999, Las Vegas, Nevada, USA, published by Los Alamos National Laboratory, LA-UR-99-4700.

Hisada Y., 1994. An efficient method for computing Green's functions for a layered halfspace with sources and receivers at close depths. *Bull. Seism. Soc. Am.* 84, 1456–1472.

Horike, M., 1985. Inversion of phase velocity of long period micro tremors to the S-wavevelocity structure down to the basement in urbanized areas, *J. Phys. Earth*, 33, 59-96.

Hough S.E., Seeber L., Rovelli A., Malagnini L., DeCesare A., Selvaggi G., and Lerner-Lam A., 1992. Ambient noise and weak motion excitation of sediment resonances: results from the Tiber Valley, Italy, *Bull. Seism. Soc. Am.*, 82, 1186-1205.

Jones R.B., 1958. In-situ measurement of the dynamic properties of soil by vibration methods. Geotechnique, 8 (1), 1-21

Kárason, H., and van der Hilst, R.D., 2001. Tomographic imaging of the lowermost mantle with differential times of refracted and diffracted core phases (PKP, Pdiff), *J. Geophys. Res.*, 106, 6569-6587

Karray, M. and Lefebvre, G., 2000. Identification and isolation of multiple modes in Rayleigh wave testing methods. *ASCE Proceedings Use of Geophysical Methods in Construction*, Geo Denver, pp. 80–94.

Kayen R., Scasserra G., Stewart J.P., Lanzo G. 2008. Shear Wave Structure of Umbria and Marche, Italy, Strong Motion Seismometer Sites Affected by the 1997 Umbria-Marche, Italy, earthquake sequence : U.S. Geological Survey, Open File Report 2008-1010, 46 pg;

Kayen R., Scasserra G., Stewart J.P., Lanzo G. 2008. Revised 2009. Shear wave structure of Umbria and Marche, Italy, strong motion seismometer sites affected by the 1997 Umbria-Marche, Italy, earthquake sequence : U.S. Geological Survey, Open-File Report 2008-1010, v. 1.1, 51 p.

Kind, F., Fäh, D., Giardini, D., 2005. Array measurements of S-wave velocities from ambient vibrations, *Geophysical Journal International*, 160, 114-126.

Kitsunezaki C., Goto N., Kobayashi Y., Ikawa T., Horike M., Saito T., Kurota T., Yamane K. and Okozumi K., 1990. Estimation of P- and S-wave velocities in deep soil deposits for evaluating ground vibrations in earthquake. J.JSNDS, 9, 1-17.

Krűger, F., Baumann, M., Scherbaum, F., and Weber, M., 2001. Mid mantle scatterers near the Mariana slab detected with a double array method, *Geophys. Res. Lett.*, 28, 667-670.

Kværna, T., 1989. On exploitation of small-aperture NORESS type arrays for enhanced Pwave detectability, *Bull. Seismol. Soc. Am.*, 79, 888-900.

Ibs-von Seht, M., and J. Wohlenberg, 1999. Microtremor measurements used to map thickness of soft sediments, *Bull. Seism. Soc. Am.* 89, 250–259.

Lacoss, R.T., Kelly, E.J., Toksöz, M.N., 1969. Estimation of seismic noise structure using arrays, *Geophysics*, 34, 21-38.

Lai C.G. and Wilmanski K. (eds), 2005. Surface waves in geomechnics: direct and inverse modelling for soils and rocks, Springer, Wien, pp. 385

Lai C.G., 1998. Simultaneous inversion of Rayleigh phase velocity and attenuation for near-surface site characterization. PhD Diss., Georgia Inst. of Techn., Atlanta (Georgia, USA)

Lai C.G. and Rix G.J., 2002. Solution of the Rayleigh eigenproblem in viscoelastic media. Bull. Seism.Soc. Am., 92(6), 2297–2309

Lai C.G., Rix G.J., Foti S., Roma V., 2002. Simultaneous Measurement and Inversion of Surface Wave Dispersion and Attenuation Curves. Soil Dynamics and Earthquake Engineering, 22 (9-12), 923-930

Lermo, J. and Chavez-Garcia, F. J., 1994 Are microtremors useful in site response evaluation?" Bull. Seism. Soc. Am. 84, 135, 1364.

Lin, F.-C., Ritwoller, M.H., Townend, J., Bannister, S. & Savage M.K., 2007. Ambient noise Rayleigh wave tomography of New Zealand, *Geophys. J. Int.,* 170, 649–666, doi:10.1111/j.1365–246X.2007.03414x.

Louie J.N., 2001. Faster, better: shear-wave velocity to 100 meters depth from refraction microtremor arrays. Bull. Seismol. Soc. Amer., 91, n.2 , 347-364.

Luzi L. and Sabetta F. (2006). Data base dei dati accelerometrici italiani relativi al periodo 1972-2004. DPC-INGV S6 Project (2004-2006), http://esse6.mi.ingv.it/ .

Lunedei E. and Albarello D., 2009. On the seismic noise wave field in a weakly dissipative layered Earth. Geophys.J.Int., DOI: 10.1111/j.1365-246X.2008.04062.x

Malagnini, L., Rovelli, A., Hough, S.E., and Seeber, L., 1993, Site amplification estimates in the Garigliano Valley, Central Italy, based on dense array measurements of ambient noise: Bull. Seism. Soc. Am., 83, 1744-1755.

Malagnini L., Herrmann R.B., Biella G., de Frando R., 1995. Rayleigh waves in quaternary alluvium from explosive sources: determination of shear-wave velocity and Q structure. Bull. of Seism. Soc. of A., 85, pp. 900-922

Maraschini M., Ernst F., Boiero D., Foti S., Socco V. 2008 Innovative multimodal inversion of surface wave data. 70th EAGE Conference, Rome, 9-12 June 2008, CD-Rom

McMechan G.A., Yedlin M.J., 1981. Analysis of dispersive waves by wave field transformation. Geophysics. 46: 869-874

Mucciarelli, M., 1998 Reliability and applicability of Nakamura's technique using microtremors: an experimental approach, J. Earthq. Engrg. 2, 625 638.

Mulargia F. and Castellaro S., 2008. Passive Imaging in Nondiffuse AcousticWavefields. Phys.Rev.Lett., 100, 218501

Nakamura, Y., 1989, A method for dynamic characteristics estimations of subsurface using microtremors on the ground surface: Q. Rept. RTRI Jpn., 30, 25-33.

Nazarian S., Stokoe II K.H., 1984. In situ shear wave velocities from spectral analysis of surface waves. Proc. 8th Conf. on Earthquake Eng. - S.Francisco, vol. 3, Prentice-Hall, pp. 31-38

Nazarian S., Desai M.R., 1993 Automated surface wave method: field testing. J. Geotechnical Eng., vol. 119 (7), ASCE, pp. 1094-1111

Nelder, J.A., and Mead, R., 1965, A simplex method for function minimization: Comp. J., 7, 308-313.

Nogoshi, M., and T. Igarashi, 1970. On the propagation characteristics of microtremors, *J. Seism. Soc. Japan* 23, 264–280 (in Japanese with English abstract).

Nogoshi, M. and Igarashi, T., 1971. On the amplitude characteristics of microtremor (Part 2). J. Seism. Soc. Japan 24, 26 40.

Okada, H., 2003. The Microtremor Survey Method. Geophys, Monograph Series, SEG, 129 pp.

Ohori, M., Nobata, A., and Wakamatsu, K., 2002. A comparison of ESAC and FK methods of estimating phase velocity using arbitrarily shaped microtremor analysis, Bull. Seism. Soc. Am., 92, 2323-2332.

O'Neill A., 2004. Full waveform reflectivity for inversion of surface wave dispersion in shallow site investigations, Proc. ISC-2 on Geotechnical and Geophysical Site Characterization, Viana da

Park C.B., Miller R.D., Xia J., 1999. Multichannel analysis of surface waves. Geophysics 64: 800-808

Parolai S, Bormann P, Milkereit C., 2001. Assessment of the natural frequency of the sedimentary cover in the Cologne area (Germany) using noise measurements. J. Earthq. Engrg. 5, 541-564.

Parolai, S., Picozzi, M., Richwalski, S.M., and Milkereit C., 2005. Joint inversion of phase velocity dispersion and H/V ratio curves from seismic noise recordings using a genetic algorithm, considering higher modes, Geoph. Res. Lett., 32, doi: 10.1029/2004GL021115.

Parolai, S., Richwalski, S.M., Milkereit, C. & Faeh, D., 2006. S-wave velocity profile for earthquake engineering purposes for the Cologne area (Germany), Bull. Earthq. Eng., 65–94, doi:10.1007/s10518-005-5758-2.

Parolai, S., Mucciarelli, M., Gallipoli, M.R., Richwalski, S.M., and Strollo, S., 2007. Comparison of Empirical and Numerical Site Responses at the Tito Test Site, Southern Italy, Bull. Seism. Soc. Am., 97, 1413-1431.

Picozzi, M., S. Parolai and D. Albarello, 2005. Statistical analysis of noise horizontal to-vertical spectral ratios (HVSR), Bull. Seism. Soc. Am.,95,1779,1786.

Picozzi, M. & Albarello, D., 2007. Combining genetic and linearized algorithms for a two-step joint inversion of Rayleigh wave dispersion and H/V spectral ratio curves. Geophys. J. Int., 169, 189–200.

Picozzi, M.; Parolai, S.; Bindi, D.; Strollo, A., 2008: Characterization of shallow geology by high-frequency seismic noise tomography, Geophysical Journal International, 176, 1, 164-174.

Poggiagliolmi E., Berkhout A.J., Boone M.M., 1982 "Phase unwrapping, possibilities and limitations", Geophysical Prospecting, vol. 30, pp. 281-291

Press, F., 1968. Earth models obtained by Monte Carlo inversion. Journal of Geophysical Research 73, 5223-5234.

Press, W.H., Teulkolsky, S.A., Vetterling, W.T., and Flannery, B.P., 1986, Numerical Recipes in Fortran 77, The Art of Scientific Computing: Cambridge University Press.

Richwalski, S.; Picozzi, M.; Parolai, S.; Milkereit, C.; Baliva, F.; Albarello, D.; Row-Chowdhury, K.; van der Meer, H.; Zschau, J., 2007: Rayleight wave dispersion curves from seismological and engineering-geotechnical methods: a comparison at the Bornheim test site (Germany), Journal of Geophysics and Engineering, 4, 349-361.

Ritter, J.R.R., Jordan, M., Christensen, U., and Achauer, U., 2001. A mantle plume below the Eifel volcanic fields, Germany, Earth Planet. Sci. Lett., 186, 7-14.

Roesset J.M., Chang D.W., Stokoe K.H., 1991 "Comparison of 2-D and 3-D models for analysis of surface wave tests", Prooc. 5th Int. Conf. on Soil Dyn. and Earthq. Eng., Kalsruhe, vol. 1, pp. 111-126

Rost, S., and Thomas, C., 2002. Array Seismology: Methods and Applications, *Reviews of Geophysics*, 40, 3.

Sabra, K.G., Gerstoft, P., Roux, P., Kuperman, W.A. & Fehler, M.C., 2005. Surfacewave tomography frommicroseisms in Southern California, *Geophys. Res. Lett.,* 32, L14311, doi:10.1029/2005GL023155.

Sànchez-Salinero I., 1987. Analytical investigation of seismic methods used for engineering applications. PhD Diss. Un. of Texas at Austin

Santamarina J.C., Fratta D., 1998. Introduction to discrete signals and inverse problems in civil engineering. Asce Press. Reston

Scherbaum, F., Hinzen, K.-G., and Ohrnberger, M., 2003. Determination of shallow shearwave velocity profiles in Cologne, Germany area using ambient vibrations, *Geophys. J. Int.*, 152, 597-612.

Schuster, G.T., 2001. Theory of daylight/interferometric imaging: tutorial, in *Proceedings of 63rd Meeting, European Association of Geoscientists and Engineers*, Session: A32 (extended Abstracts).

Schuster, G.T., Yu, J., Sheng, J. & Rickett, J., 2004. Interferometric/daylight seismic imaging, *Geophys. J. Int.,* 157, 838–852.

SESAME, 2003. Final report on measurements guidelines, LGIT Grenoble, CETE Nice,WP02, H/V technique:experimental conditions, http://sesame-fp5.obs.ujf-grenoble.fr/Delivrables/D08-02_Texte.pdf

Shapiro, N.M. & Campillo, M., 2004. Emergence of broadband Rayleigh waves from correlations of the ambient seismic noise, *Geophys. Res. Lett.,* 31, L07614, doi:10.1029/2004GL019491.

Shapiro, N.M., Campillo, M., Stehly, L. & Ritzwoller, M., 2005. High resolution surface wave tomography from ambient seismic noise, *Science,* 307, 1615–1618.

Snieder, R., Scattering of surface waves , in *Scattering and Inverse Scattering in Pure and Applied Science*, Eds. Pike, R. and P. Sabatier, Academic Press, San Diego, 562-577, 2002

Snieder, R., 2004. Extracting the Green's function from the correlation of coda waves: a derivation based on stationary phase, *Phys. Rev. E,* 69, doi:10.1103/PhysRevE.69.046610.

Socco, L.V. and Strobbia, C., 2004 Surface Wave Methods for near-surface characterisation: a tutorial. Near Surface Geophysics 2(4), 165-185.

Socco L.V., Boiero D., 2008. "Improved Monte Carlo inversion of surface wave data", Geophysical Prospecting, Volume 56 Issue 3, Pages 357 – 371.

Socco L.V., Boiero D., Foti S., Wisén R., 2009. "Laterally constrained inversion of ground roll from seismic reflection records", Geophysics, SEG, in press

Stephenson, W.J., Louie, J.N., Pullammanappallil, S., Williams, R.A., and Odum, J.K., 2005. Blind Shear-wave velocity comparison of ReMi and MASW results with boreholes to 200 m in Santa Clara Valley: implication for earthquake ground motion assessment. *Bull. Seism. Soc. Am.*, 95, 2506-2516.

Stokoe K.H. II, Wright S.G., J.A. Bay, J.M. Roesset., 1994. Characterization of geotechnical sites by SASW method. Geophysical Characterization of Sites. R.D. Woods Ed.: 15-25.

Strollo, A.; Parolai, S.; Jäckel, K.-H.; Marzorati, S.; Bindi, D. 2008. Suitability of Short-Period Sensors for Retreiving Reliable H/V Peaks for Frequencies Less Than 1 Hz, *Bull. Seism. Soc. Am.*, 98, 2, 671-681.

Szelwis R., Behle A., 1987. Shallow shear-wave velocity estimation from multimodal Rayleigh waves, in Danbom, S. and Domenico, S. N., Ed., Shear-wave exploration: Soc. Expl. Geophys., pp.214-226

Tarantola A., 2005 Inverse problem theory and methods for model parameter estimation. Siam, Philadelphia, 1-55.

Thorson, J. R., and J. F. Claerbout, 1985. Velocity-stack and slant-stack stochastic inversion, *Geophysics* 50, 2727–2741.

Tokimatsu, K., Kuwayama, S., Tamura, S., and Miyadera, Y., 1991, Vs determination from steady state Rayleigh wave method: Soils and Foundations, 31, 153-163.

Tokimatsu, K., S. Tamura, and H. Kojima, 1992. Effects of multiple modes on Rayleigh wave dispersion characteristics. *Journal of Geotechnical Engineering* 118, 1529–1543.

Tokimatsu K., 1995 Geotechnical Site Characterisation using Surface Waves. Proc. IS Tokyo 1995, Balkema, 1333-1368

Tselentis G-A., Delis G, 1998. Rapid assessment of S-wave profiles from the inversion of multichannel surface wave dispersion data. Annali di Geofisica. 41. 1-15

Van der Sluis, A., and Van der Vorst, H.A., 1987, Numerical solution of large sparse linear algebraic system arising from tomographic problems, *in* Seismic Tomography, edited by G. Nolet: D. Reidel, pp. 49-83, Norwell, Mass.

Wapenaar, K., 2004. Retrieving the elastodynamic Green's function of an arbitrary inhomogeneous medium by cross correlation, *Phys. Rev. Lett.,* 93, 25 4301–1-4.

Wapenaar, K. & Fokkema, J., 2006. Green's function representations for seismic interferometry, *Geophyscis,* 71, SI33–SI44.

Weaver, R.L. & Lobkis, O.I., 2001. Ultrasonics without a source: thermal fluctuation correlation at MHz frequencies, *Phys. Rev. Lett.,* 87, 134301–134304.

Weaver, R.L. & Lobkis, O.I., 2004. Diffuse fields in open systems and the emergence of the Green's function, *J. acoust. Soc. Am.,* 116, 2731–2734.

Whiteway, F.E., 1966. The use of arrays for earthquake seismology, *Proc. R. Soc. London*, Ser. A, 290, 328-348.

Xia, J., Miller, R.D., and Park, C.B., 1999, Estimation of near-surface shear wave velocity by inversion of Rayleigh waves: Geophysics, 64, 733-741.

Yang, Y., Ritzwoller, M.H., Levshin, A.L. & Shapiro, N.M., 2007. Ambient noise Rayleigh wave tomography across Europe, *Geophys. J. Int.,* 168, 259–274, doi:10.1111/j.1365–246X.2006.03203.x

Yamanaka, H., M. Takemura, H. Ishida, and M. Niwa, 1994. Characteristics of long-period microtremors and their applicability in the exploration of deep sedimentary layers, *Bull. Seism. Soc. Am.* 84, 1831–1841.

Yamanaka, H., and Ishida, H., 1996. Application of Generic algorithms to an inversion of surface-wave dispersion data. *Bull. Seism. Soc. Am*. 86, 436-444.

Yao, H., Van Der Hilst, R.D. & De Hoop, M.V., 2006. Surface-wave array tomography in SE Tibet from ambient seismic noise and two station analysis: I—phase velocity maps, *Geophys. J. Int.,* 166, 732– 744.

Yaramanci, U., Lange, G. & Hertrich, M., 2002. Aquifer characterisation using Surface NMR jointly with other geophysical techniques at the Nauen/Berlin test site, *J. Appl. Geophys.,* 50, 47–65.

Yokoi, T. & Margaryan, S., 2008. Consistency of the spatial autocorrelation method with seismic interferometry and its consequence, *Geophys. Prosp.,* 56, 435–451.

Zhang, S.X. and L.S. Chan, 2003. Possible effects of misidentified mode number on Rayleigh wave inversion. *Journal of Applied Geophysics* 53, 17–29.

Zhang, S.H., Chan, L.S. and Xia, J., 2004. The selection of field acquisition parameters for dispersion images from multichannel surface wave data. *Pure and Applied Geophysics* 161, 185–201.

Zywicki, D.J., 1999. Advanced Signal Processing Methods Applied to Engineering Analysis of Seismic Surface Waves. PhD thesis at Georgia Institute of Technology

9. Key publications/presentation

Tokeshi K., Foti S., Parolai S., Picozzi M., Puglia R., Massa M., D'Alema E., 2009. Love and Rayleigh waves dispersion analysis from microtremor measurements at Bevagna (Italy). Abstract presented at the Workshop on Surface wave analysis for exploring at different scales, EAGE09, Amsterdam, 7 June 2009

Comina C., Foti S., Maraschini M., 2009. Multimodal Inversion of Surface Wave Data at Sites with Shallow Bedrock. Abstract presented at the Workshop on Surface wave analysis for exploring at different scales, EAGE09, Amsterdam, 7 June 2009

ANNEX

Updated list of sites to be investigated (see http://esse4.mi.ingv.it/ Task3 for further details)

COD	Station Name	Province	Region	Site	Owner	Lat°	Long°	Alt [m]	Itype	# rec
LGN	Lagonegro	Potenza	Basilicata	stiff soil	attiva	40.1311	15.7585	809	D	4
GRM	Grumento Nova	Potenza	Basilicata		attiva	40.3103	15.8853		A	3
SNA	Sant'Arcangelo	Potenza	Basilicata		attiva	40.2580	16.2350		D	1
ARG	Argenta	Ravenna	Emilia R.	soft soil	attiva	44.6307	11.8252		D	0
FAZ	Faenza	Ravenna	Emilia R.	soft soil	attiva	44.2960	11.8920	75	D	5
CTL	Cattolica	Rimini	Emilia R.	soft soil	attiva	43.9550	12.7359		D	0
NVL	Novellara	Reggio Emilia	Emilia R.	soft soil	attiva	44.8419	10.7306	23	A	4
MDN	Modena	Modena	Emilia R.	soft soil	attiva	44.6470	10.8899	37	D	2
BZZ	Bazzano	L'Aquila	Abruzzo	soft soil	attiva	42.3370	13.4686		D	
NOR	Norcia	Perugia	Umbria	soft soil	attiva	42.7920	13.0920	662	D	>100
RNS	RONCO SCRIVIA	Genova	Liguria	rock	attiva	44.6128	8.9484		D	0
SEL	SESTRI LEVANTE	Genova	Liguria	rock	attiva	44.2731	9.3968		D	0
GNV	GENOVA	Genova	Liguria	rock	attiva	44.4071	8.9340		D	0
VRL	VARESE LIGURE	La Spezia	Liguria	rock	attiva	44.3774	9.5953		D	0
TRT	TORTONA	Alessandria	Piemonte	stiff soil	attiva	44.8925	8.8825	210	A	1
PNR	PINEROLO	Torino	Piemonte	stiff soil	attiva	44.8778	7.3444	355	A	1
CLG	CALTAGIRONE	Catania	Sicilia	stiff soil	attiva	37.2116	14.5208	531	D	7+1
PTT0	PATTI (CAB. ENEL)	Messina	Sicilia	stiff soil	attiva	38.1344	14.9751		D	13+5
TOR	TORTORICI	Messina	Sicilia	rock	attiva	38.0440	14.8146	554	D	6+2
ISI	ISPICA	Ragusa	Sicilia	rock	attiva	36.7978	14.8924	276	D	4+2
NTE	NOTO	Siracusa	Sicilia	rock	attiva	36.9096	15.0692	235	D	6
TRF	TORRE FARO (MESSINA) (CAB. ENEL)	Messina	Sicilia	stiff soil	attiva	38.2643	15.6342	3	D	7
PLZ	PALAZZOLO ACREIDE	Siracusa	Sicilia	rock	attiva	38.0680	15.9090	658	D	8+2
GEA	GELA	Caltanissetta	Sicilia	stiff soil	attiva	37.0563	14.3145		D	
SCR	S. CROCE CAMERINA	Ragusa	Sicilia	rock	attiva	36.8297	14.5276		D	
RGS	RAGUSA	Ragusa	Sicilia	rock	attiva	36.9248	14.7033		D	
PCH	PACHINO	Ragusa	Sicilia	rock	attiva	36.7108	15.0911		A	
CAT	CATANIA - PIANA	Catania	Sicilia	stiff soil	attiva	37.4469	15.0467		A	10
AQA	AQUILA FIUME ATERNO	L'Aquila	Abruzzo	stiff soil	attiva	42.3755	13.3393	693	D	18
AVZ	Avezzano	L'Aquila	Abruzzo	stiff soil	attiva	42.0275	13.4259	746	D	6+9
BTT2	Borgo Ottomila	L'Aquila	Abruzzo	soft soil	dismessa	41.9983	13.5431	652	D	3
CSS	Cassino		Lazio		attiva	41.5231	13.8636		D	2+9
RTI	Rieti	Rieti	Lazio	soft soil	attiva	42.4303	12.8211	380	D	6
BBN	Bibbiena	Arezzo	Toscana		attiva	43.7476	11.8214	471	D	1
DCM	Dicomano	Firenze	Toscana		attiva	43.8912	11.5180	157	D	0
CPS	CAPESTRANO	L'Aquila	Abruzzo	Rock	attiva	42.2720	13.7580	585	D	16
SCN	SCANNO	L'Aquila	Abruzzo	Rock	attiva	41.9187	13.8724	985	D	1
VBM	VIBO MARINA	Vibo Valentia	Calabria	soft soil	attiva	38.7138	16.1232	56	D	1
VBV	VIBO VALENTIA	Vibo Valentia	Calabria	stiff soil	attiva	38.6779	16.1065	546	D	10
ATN	ATINA	Frosinone	Lazio	Rock	attiva	41.6203	13.8014	440	A	2
MTC	MONTECASSINO (CASSINO)	Frosinone	Lazio	Rock	attiva	41.4903	13.8128	512	A	1
PSC	Pescasseroli	L'Aquila	Abruzzo	Rock	attiva	41.8120	13.7892	1242	D	15
AQP	Aquila Pettino	L'Aquila	Abruzzo		attiva	42.3837	13.3686	1193	D	18
SGIU	S.Giuliano Aquila	L'Aquila	Abruzzo		attiva	42.3730	13.3920		D	2
COS	Cosenza	Cosenza	Calabria		attiva	39.2891	16.2577	376	D	5
MRM	Mormanno	Cosenza	Calabria		attiva	39.8832	15.9896	919	D	2
NCO	Nicotera (scuola)	Vibo Valentia	Calabria		attiva	38.5530	15.9380	271	D	0
PMI	Palmi	Reggio Calabria	Calabria		attiva	38.3554	15.8533	340	D	0
SGV	S.Giovanni in Fiore	Cosenza	Calabria		attiva	39.2633	16.6898	1166	D	2
SCI	Scilla	Reggio Calabria	Calabria		attiva	38.2558	15.7147	81	D	1
SPS	Spezzano della Sila (Camigl.)	Cosenza	Calabria		attiva	39.3402	16.4491	1305	D	4
VLS2	Villa S.Giovanni	Reggio Calabria	Calabria		attiva	38.2176	15.6470	144	D	5
LSS	Leonessa	Rieti	Lazio		attiva	42.5582	12.9689	1065	D	7
MMP	Mompeo	Rieti	Lazio		attiva	42.2486	12.7486	474	D	6
SBS	Subiaco	Roma	Lazio		attiva	41.9132	13.1055	680	D	7
TRO	TRICARICO	Matera	Basilicata	Rock	attiva	40.6146	16.1422	770	D	
MRV	MARSICO VETERE	Potenza	Basilicata	rock	attiva	40.3614	15.8265	747	D	9
MLF	MELFI	Potenza	Basilicata	stiff soil	attiva	40.9971	15.6460		D	
PGA	PIGNOLA	Potenza	Basilicata	rock	attiva	40.5686	15.7789	1018	D	
PTZ	POTENZA	Potenza	Basilicata	stiff soil	attiva	40.6482	15.8081	766	D	10
STL	SATRIANO DI LUCANIA	Potenza	Basilicata	stiff soil	attiva	40.5408	15.6431	748	D	4
MRA	MARATEA	Potenza	Basilicata	Rock	attiva	39.9871	15.7309	535	D	